which will be discussed further below. Also, the well-known singlet high energy transition, the Soret band, was found at 413 nm. Regarding to the Q bands, the characteristic D_{2h} symmetry of the porphyrin in this work reflects their splitted four-banded absorption spectrum in the Q-band region.[84] All the spectral features are organized in Table 2.1.

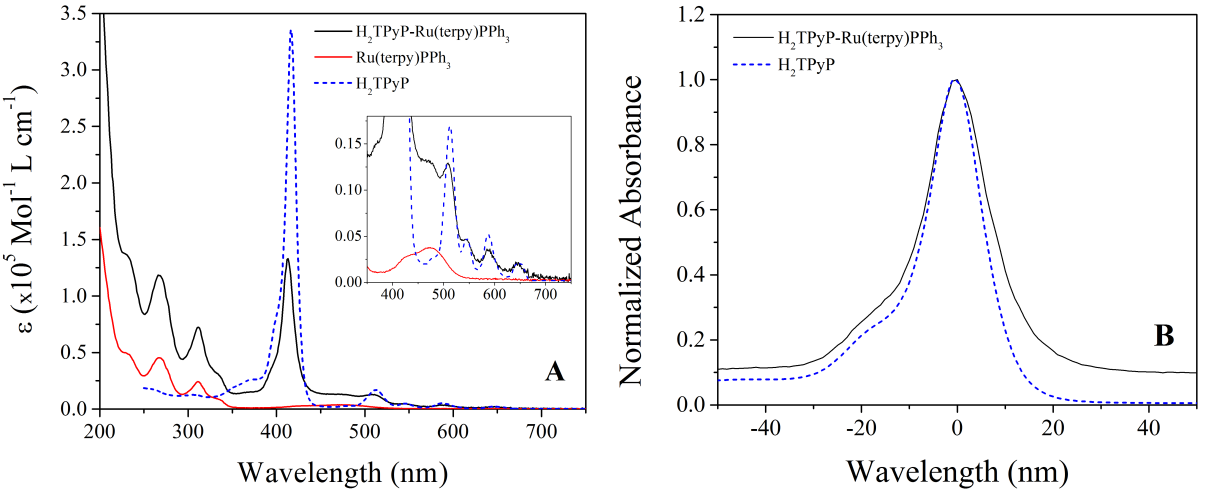

Figure 2.2. (A) Steady-state UV-Vis absorbance spectrum of H_2TPyP-Ru(terpy)PPh_3 (black), Ru(terpy)PPh_3 (red) and H_2TPyP (blue) in dichloromethane. The inset shows the rescaled spectra for better visualization in the range of 350 nm to 700 nm. (B) To verify the broadening of the Soret band, the absorbance spectra of H_2TPyP-Ru(terpy)PPh_3 and H_2TPyP were normalized and centralized to zero, for the sake of comparison.

Table 2.1. UV-Vis absorption spectra features of H_2TPyP-Ru(terpy)PPh_3, Ru(terpy)PPh_3 and H_2TPyP in dichloromethane.

	UV-vis absorption λ_{MAX} (nm)									
	Ru component					Porphyrin component				
						Soret Band	Q-band			
Ru(terpy)PPh_3	230	268	311	334	470					
H_2TPyP						416	510	545	587	645
H_2TPyP-Ru(terpy)PPh_3	230	268	311	334	470	413	510	545	587	645

In order to better understand the influence of the peripheral ruthenium groups in the H_2TPyP-Ru(terpy)PPh_3 absorption spectrum, the free base tetrapyridil porphyrin, H_2TPyP, was taken for comparison, Figure 2.2A. The difference between them is remarkable in almost all the UV and visible range. The solely H_2TPyP does not show significant absorption features at the UV region, and it also has a characteristic energy gap between the Soret band and the Q-band, 440 – 490 nm.

Comparing the spectra in Figure 2A, the UV region of Ru(terpy)PPh_3 has been ascribed to intraligand $\pi \rightarrow \pi^*$ transitions within both the terpyridine (terpy) and the triphenylphosphine ligands (PPh_3).[81, 85-87] In the visible region, the lower energy absorption bands were assigned to metal-to-ligand charge transfer (MLCT) transitions which are predominantly Ru($d\pi$) $\rightarrow$ terpy(π^*), in analogy to other reported works.[88] Furthermore, previous work have established categories to the structuration of the Q-bands based on perturbation by external substituents.[84, 89-90] Although the ruthenium moiety enhances the overall absorbance of H_2TPyP-Ru(terpy)PPh_3 between 400 nm and 550 nm, by subtraction it is possible to ensure that the intensity of the porphyrin Q-band absorption spectrum is preserved. It's worth noting that extinction coefficients due to the ruthenium outlying groups were in a 4:1 proportion relative to the porphyrin ring. Consequently, the observed extra features in the absorption spectrum of H_2TPyP-Ru(terpy)PPh_3, below 390 nm and in between of 450 nm and 550 nm, were essentially attributed to the overlapping of those belonging to the Ru(terpy)PPh_3 outlying substituents. The results suggested that the external complexation with the ruthenium groups did not significantly perturbed the porphyrin lowest singlet excited state, S_1, maintaining the *phyllo* type for the Q bands relative intensity.

While the Q bands did not seemed to be affected by the ruthenium groups, the Soret band, instead, exhibited major changes that could not be explained simply by overlapping and sum of individual contributions. It was observed significant decrease in the oscillator strength and also the broadening of the Soret band, Figure 2.2A and B. As previously reported, the observed broadening of the Soret band is a clear consequence of new vibrational modes being activated after the complexation of H_2TPyP with the Ru(terpy)PPh_3 groups. However, up to our knowledge, there is no established explanation to the decrease of the Soret band oscillator strength. Similar results have also been reported.[91]

Such findings can indicate that the outlying ruthenium groups mainly interact with the second excited singlet state. Probably the molecular orbitals giving rise to the Q band do not involves the pyridine ligands while he S_2 excited state may overlap orbitals of both individual components.

PL experiments on Ru(terpy)PPh_3 revealed it has two weak emission bands centered at 545 nm and 625 nm, Figure 2.3A. The substituted porphyrin exhibited very similar photoluminescence spectral features with the unsubstituted H_2TPyP,[13] with peaks at 650 nm and 711 nm. Additionally, a very weak signal was observed at wavelengths lower than 600 nm, which is unusual for most of regular porphyrins, Figure 2.3B. These extra bands were assigned to the emission originated in the peripheral ruthenium moieties. Their very low

signal was due to the low concentration of the porphyrin solution used to excite directly at the Soret band maximum absorption band, and to the significantly low photoluminescence quantum yield of the ruthenium moiety. When overlaid and normalized to the 545 nm wavelength, it is clearly seen that the extra photoluminescence signal was due to the overlapping of a multiple and independent photoluminescent sites, the porphyrin ring and the external ruthenium moieties.

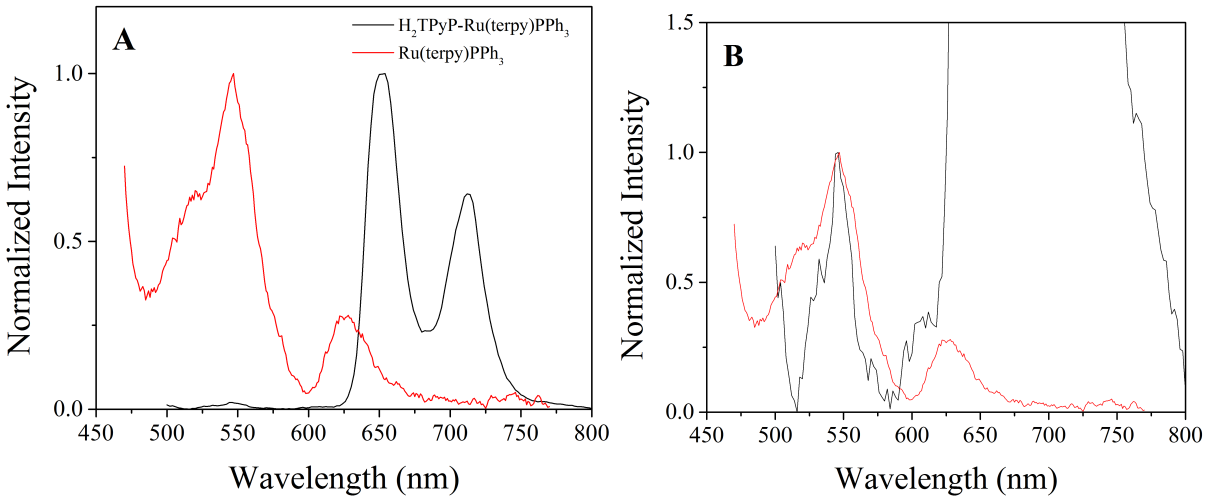

Figure 2.3. Normalized steady-state photoluminescence of H_2TPyP-Ru(terpy)PPh_3 (black) and Ru(terpy)PPh_3 (red) in dichloromethane, excited at 470 nm. (A) normalizes the spectra at the emission maximum peak, while (B) normalizes the spectra at 545 nm.

The hypothesis that the H_2TPyP-Ru(terpy)PPh_3 photoluminescence is a result of the overlap between a stronger signal from the porphyrin ring and a second and less intense emission originated at the Ru(terpy)PPh_3 groups, could be confirmed by simply taking the excitation spectra of the substituted porphyrin, Figure 2.4. Excitation spectra by monitoring the porphyrin emission peak at 650 nm accurately retrieved the unsubstituted H_2TPyP porphyrin absorption spectrum. While probing the emission at 545 nm exclusively recovered the visible range of the Ru(terpy)PPh_3 absorption spectrum. This result supported the idea that both moieties might be interacting independently upon light interaction, expressed through their steady state photophysical properties. Although linked, both compounds did not show intramolecular interactions such as electron transfer. Probably some minor perturbations can be found with more specific experiments and data analysis.

Generally, heteroleptic ruthenium(II) polypiridyl complexes exhibit photoluminescence from triplet excited states with lifetime from hundreds of nanoseconds to tens of microseconds associated with the deactivation of thermalized tripled excited states to

the ground state.[92-93] Time-resolved photoluminescence on $Ru(terpy)PPh_3$ revealed that the excited state lifetime was bi-exponential with one subnanosecond component and a second component of 3 ns. These measured lifetimes are much faster than the expected. Most of the heteroleptic ruthenium compounds have high quantum yield of triplet state formation and high intersystem crossing rates.[92-93] So, the nearly formed triplet excited states were rapidly deactivated through either fast radiative or non-radiative pathways back to the ground state, S_0.

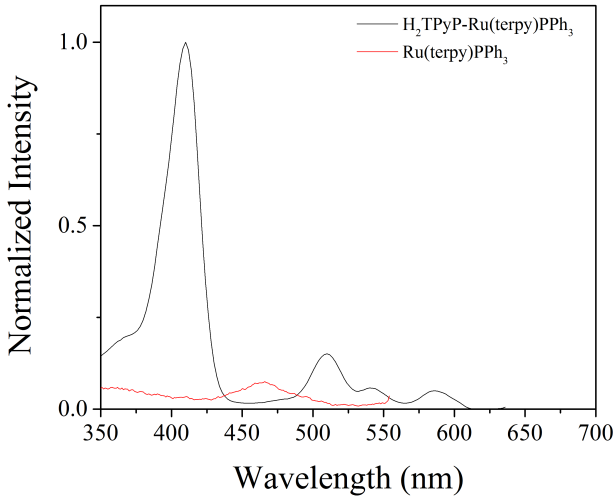

Figure 2.4. Excitation spectra of H_2TPyP-$Ru(terpy)PPh_3$ (black) probing the emission at 650 nm; and $Ru(terpy)PPh_3$ (red) in dichloromethane probing at 545 nm.

2.3.2 – The Absence of Intramolecular Charge Transfer Interactions.

Previous work have reported the H_2TPyP excited state lifetime to be ~8 ns and well fitted with a monoexponential decay function. This decay is associated with the depopulation of singlet excited states back to the ground state, $S_0 \leftarrow S_1$.[13] Here, when complexed with the $Ru(terpy)PPh_3$ groups, the H_2TPyP-$Ru(terpy)PPh_3$ porphyrin reveals now a fast, subnanosecond, characteristic lifetime in additional to the well known unsubstituted free base porphyrin lifetime, Figure 2.5. The performed time-resolved photoluminescence experiment revealed that the H_2TPyP-$Ru(terpy)PPh_3$ excited state is deactivated predominantly (70 %) by a fast subnanosecond process, $\tau_1 = 0.4$ ns, while the regular H_2TPyP excited state lifetime of 8 ns contributes to 30 % of its depopulation. The origin of such a faster component might be related to the enrichment of non-radiative pathways back to the ground state resulted from extra vibrational modes. Such possibility is corroborated by the fact that the insertion of the

outlying groups implied in an enlargement of the Soret-bandwidth, which can be explained as being due to the creation of new vibrational modes, favoring the dissipation of energy in nonradiative ways.

Additionally, the calculated photoluminescence quantum yield of 0.45% is 3.8 times smaller than that reported for the unsubstituted H_2TPyP (1.7%).[13] This latter observation shows that the external ruthenium groups worked as quenchers to the porphyrin excited state, where the quenching mechanism might be strongly coupled with the induced new vibrational modes. The time-resolved parameters and photoluminescence quantum yields are shown in Table 2.2.

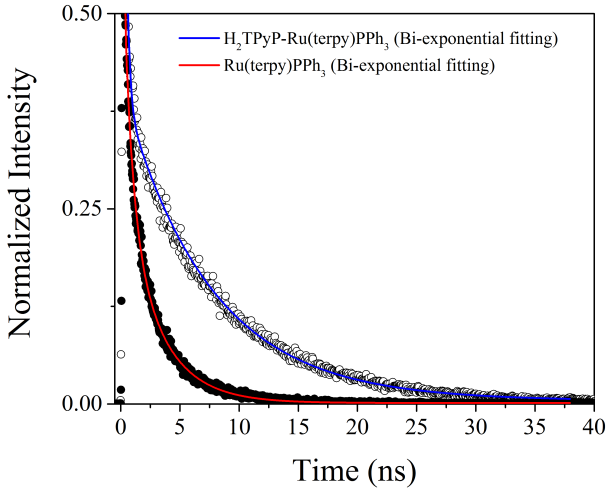

Figure 2.5. Time-resolved photoluminescence of H_2TPyP-Ru(terpy)PPh_3 (open circles) and Ru(terpy)PPh_3 (solid circles) with excitation wavelength at 460 nm, with their respective multi-exponential fitting.

Table 2.2. Multi-exponential parameters an emission quantum yield of H_2TPyP-Ru(terpy)PPh_3 and Ru(terpy)PPh_3 in dichloromethane.

Compound	τ_1 (ns)	τ_2 (ns)	ϕ (%)
H_2TPyP-Ru(terpy)PPh_3	0.4 (0.67)	7.9 (0.33)	0.45
Ru(terpy)PPh_3	0.64 (0.61)	3.0 (0.39)	-----

The values in parentheses denote the associated weight of each lifetime.

Nanosecond transient absorption experiments for a great variety of porphyrins have mainly revealed the triplet state dynamics.[13-15, 71, 75] The transient absorption spectrum of a free base tetrapyridyl porphyrin shows a characteristic bleach of the ground state between 400 nm and 430 nm, and a growth from 430 nm to 500 nm. In transient absorption, a growth signal represents an increase in absorption, and generally for porphyrins, this is assigned to the triplet excited state absorption, $T_1 \rightarrow T_n$, Figure 2.6. The results showed clear similarity

between the transient absorption spectral shape of H_2TPyP and H_2TPyP-Ru(terpy)PPh_3 spectra. Although, in a closer analysis, some differences could be pointed out: 1) For H_2TPyP-Ru(terpy)PPh_3 the ground state bleach of the Soret band was broader and 2) its relative intensity (with the growth peak) was smaller, 3.5, against 5.7 for H_2TPyP; 3) the kinetic traces for all probed wavelengths were much longer lived for H_2TPyP-Ru(terpy)PPh_3 than it was for the unsubstituted porphyrin. While the first two observations were connected with spectral shape of the stead state UV-vis absorption spectra, the later told us that the ruthenium groups changed the kinetics of the porphyrin decay pathways in both the singlet excited state previously discussed, and triplet excited states.

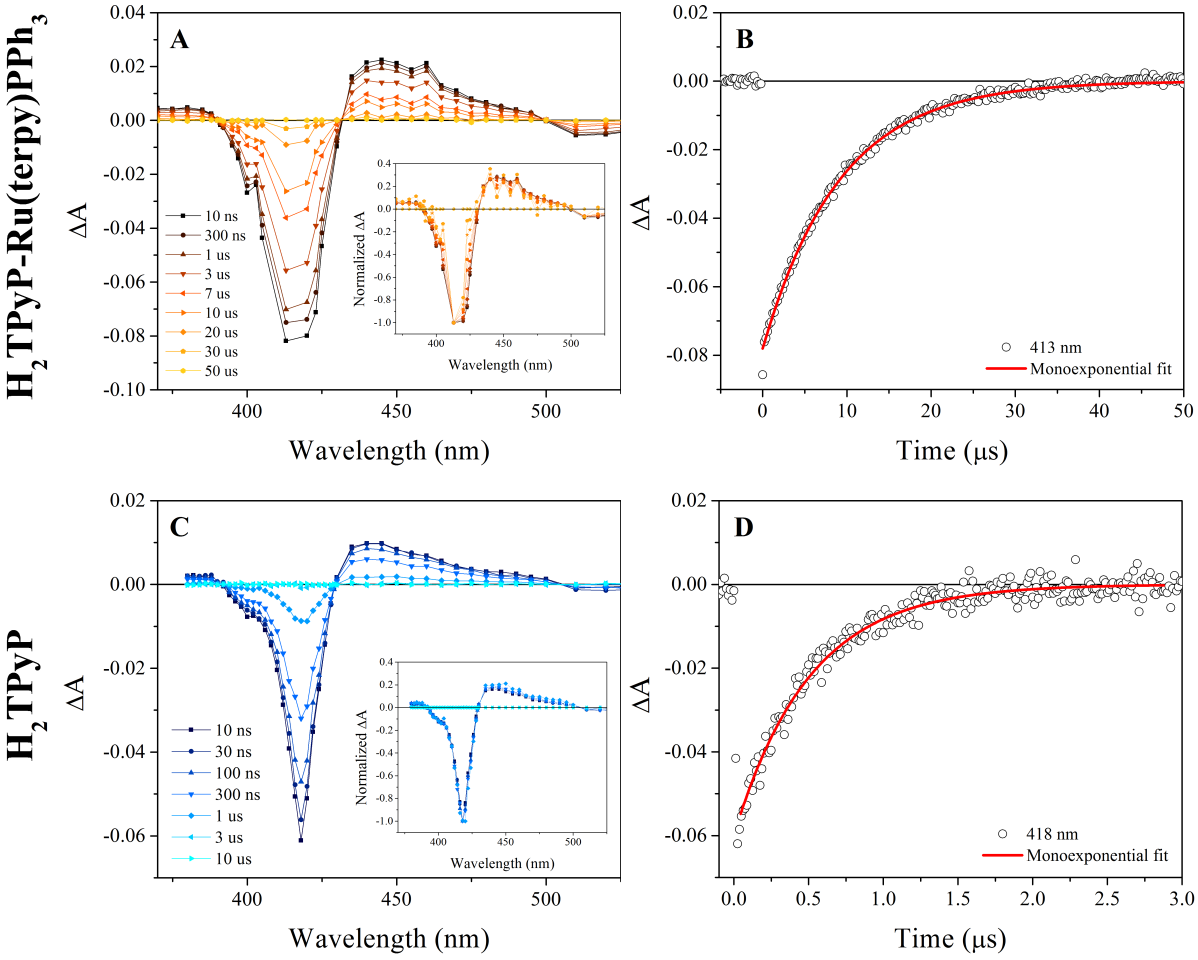

Figure 2.6. (A) Transient absorption spectra obtained over a 30 ns – 50 μs time window after pulsed 532 nm excitation of H_2TPyP-Ru(terpy)PPh_3 in dichloromethane. (B) Single wavelength transient absorption kinetic data of H_2TPyP-Ru(terpy)PPh_3 in dichloromethane, observed at 413 nm. Overlaid in red is the fit to the monoexponential function with τ = 9 μs. (C) and (D) represent the transient absorption spectra and the single wavelength transient absorption kinetics of the unsubstituted H_2TPyP porphyrin in dichloromethane. Overlaid in red is the monoexponential fit given a decay lifetime of 0.6 μs.

The measured transient triplet excited state lifetime were about 15-fold longer for H_2TPyP-Ru(terpy)PPh_3 (9 μs) than it is observed of H_2TPyP (0.6 μs). Previous work[13] have reported that the peripheral complexation of H_2TPyP with ruthenium groups is deleterious to the triplet state population, $S_1 \rightarrow T_1$, evidenced by an increase in the intersystem crossing time, τ_{ISC}. The later behavior is contrary to that observed when a metal replaces the hydrogen atoms to stabilize the porphyrin ring. Also, in the current work, an expressive increase in the triplet state lifetime, τ_T, is observed when a ruthenium triphenylphosphine is linked to the pyridines of the H_2TPyP. Specific experiments to abstract τ_{ISC} were not performed in this work, but the trend in the increase of τ_T after the ruthenium complexation was observed. Also, the fact that 70% of the S_1 excited state deactivates via a subnanosecond process, is an indirect probe to reinforce that the triplet excited state was substantially quenched by faster deactivations pathways from the first singlet excited state. It wasn't observed transient absorption signal for Ru(terpy)PPh_3 under same experimental conditions and on the nanosecond time scale.

Finaly, cyclic voltammetry was performed on the two compounds presented in this work with applied reserve (positive) bias, Figure 2.7. The Ru(terpy)PPh_3 presented formal reduction potential, E^0, of 1064 mV *vs* NHE, where the observed waves were consistent with the formation of Ru^{III} upon oxidation of Ru^{II}. The free base tetrapyridyl porphyrin containing the peripheral ruthenium groups showed very similar result as the Ru(terpy)PPh_3. The reduction potential was measured to be 1132 mV *vs* NHE and again was assigned as the equilibrium potential ($E_{1/2}$) where the concentration of Ru^{III} and Ru^{II} were equal, rather than the oxidation of the porphyrin ring. The comparison of the two cyclic voltammetry revealed that the porphyrin ring weakly affects the overall redox properties of the ruthenium groups. The more positive Ru(III/II) reduction potentials of the H_2TPyP-Ru(terpy)PPh_3 molecule, when compared with the single Ru(terpy)PPh_3 complex, suggested that the electron-withdrawing characteristic of the pyridines stabilize the dπ levels of the Ru^{2+}, lowering down its orbital energy. It is known that the energy necessary to remove one electron from the molecule ground state configuration (*i. e.* to oxidize it) is directly associated with to HOMO energy.

Oxidation of the porphryin ring was not observed in cyclic voltammetry, even at further positive potentials. Performing DFT calculations to obtain the porphyrin HOMO energy, which could simulate the ring first oxidation potential, approximately fulfilled this limitation. The calculated value was at about -6 eV, relative to the vacuum energy.

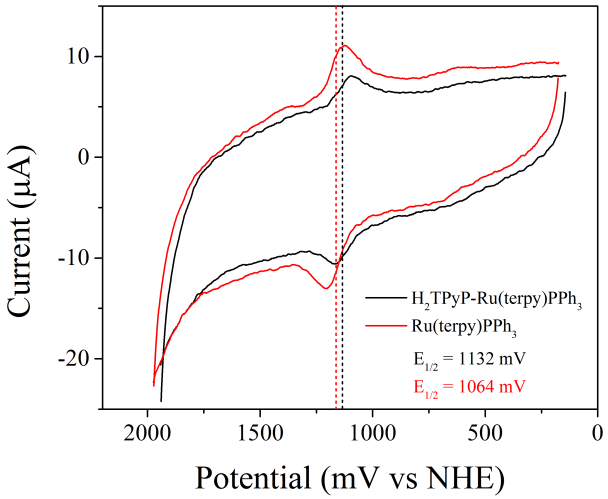

Figure 2.7. Cyclic voltammetry of H_2TPyP-Ru(terpy)PPh_3 (black) and Ru(terpy)PPh_3 (red) in Ar-purged 0.1 M TBA(PF_6) dichloromethane electrolyte solution.

The reduction potential diagram, Figure 2.8, is an important and complementary tool when studying electron transfer processes. Associated with transient absorption experiments, the diagram can predict the existence or absence of electron transfer. The following diagram was constructed using cyclic voltammograms of H_2TPyP-Ru(terpy)PPh_3 in 0.1M TBA(PF_6) electrolyte solution in dichloromethane, in which the formal reduction potentials of oxidation and reduction of the ruthenium moiety were obtained. With regards to the porphyrin ring, its reduction potential as an electron acceptor was abstracted from cyclic voltammetry while the ring oxidation was estimated from the DFT calculated HOMO energy of a free base tetrapyridyl porphyrin.

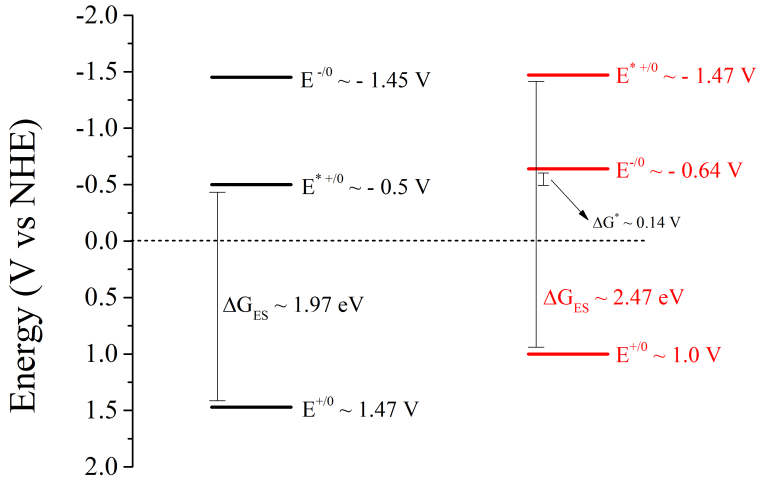

Figure 2.8. Reduction potential diagram for electron transfer processes of H_2TPyP- Ru(terpy)PPh_3. The black lines are potentials associated with the porphyrin ring while the red lines are the potentials for the Ru(terpy)PPh_3 moiety, in dichloromethane.

Transient absorption kinetics of H_2TPyP-Ru(terpy)PPh_3 showed mono-exponential behavior and the spectra were fully normalized, results that converge to the single transient process of triplet excited state formation. The spectral shape observed in Figure 2.6 have similar characteristics reported in many other works.[15, 94-95] In the reduction potential energy diagram, Figure 2.8, electron transfer from the porphyrin ring to the ruthenium complex is an uphill reaction and thus not favorable. Electron transfer from Ru(terpy)PPh_3 to the porphyrin ring has very small driving force, which, from Marcus theory for electron transfer processes, would be associated to small rate constants, or longer life-times.[96] Excited state deactivation of Ru(terpy)PPh_3 , Table 2.2, might be fast enough to efficiently kill electron transfer processes.

2.4. CONCLUSIONS

In this work, was performed steady state and time-resolved spectroscopy, and electrochemical experiments to compare the photophysical properties of the free base tetrapyridil porphyrin (H_2TPyP) when ruthenium groups are externally linked to it. Stead state spectroscopy revealed that absorption and emission spectra were independent to their specific origins, the H_2TPyP porphyrin moiety and the Ru(terpy)PPh_3 complex. However, when time-resolved experiments were employed, significant changes were observed in the H_2TPyP-Ru(terpy)PPh_3 porphyrin photophysical properties. It was seen that the complexation creates new vibrational modes between the first singlet excited state and the ground state that can be easily accessed through a fast deactivation process. The later suggests that triplet excited states were strongly quenched by the presence of outlying ruthenium groups. Also, as seen in previous work[13], the triplet excited state lifetime, τ_T, suffered an increasement when compared with the unsubstituted H_2TPyP. Electrochemical experiments provided that the ruthenium(II) ($d\pi$) orbital is stabilized when linked to the pyridines of the H_2TPyP, evidenced by a 68 mV vs NHE shift to less positive potentials of the Ru(III/II) reduction potential. Finally, although the H_2TPyP-Ru(terpy)PPh_3 compound could have strong light harvesting, the absence of intramolecular charge transfer between the two groups is not favorable to sensitization in DSSCs. The results found in this work revealed good insights about appropriate molecular

engineer linking porphyrins and ruthenium compounds. The presence of metal ions as central substituent in the porphyrin ring could modify the porphyrin energy levels and excited state dynamics so that the porphyrin ring can communicate more efficiently with the outlying ruthenium groups. If succeeded, such modified molecular structures could be a good candidate for better light harvesting and photoinjection in DSSCs.

PART II:

Sensitization of Mesoporous TiO_2 Thin Films With a Free Base Tetrapyridyl Porphyrin With Peripheral Ruthenium Groups.

INTRODUCTION

The Dye Sensitized Solar Cell

Since the prediction that fossil fuels would be completely dried up in a near future, an emerging need for new sources of energy started to motivate researches to pursue potential alternatives to fulfill the world energy needs. The necessity to develop economically viable renewable energy sources is fundamental to achieve sustainability in a globally society. The global energy consumption in the year 2000 was 13 TW and estimatives predicts this value to be 28 TW in 2050 for the global energy demand.[97-98] The solar energy is definitely one of the largest potentially promising source to satisfy the future global need for renewable energy sources, since 1.7×10^5 TW of solar energy strikes the Earth's surface per year.[99] If 0.13% of the Earth were covered with solar cells with an efficiency of 10%, the generated energy would satisfy our present needs.[100]

At the end of last century, the possibility to develop photoelectrochemical cell devices for solar electricity production based on molecules as light harvest agent seemed unlikely to happen. This concept started to change when O'Regan an Grätzel proposed, in 1991, the clever idea of utilizing mesoporous thin films of nanocrystalline TiO_2 sensitized with dye molecules in photoelectrochemical cells, Figure II-1.[101] The idea was the starting point to encourage researches on this ascending new research field of the dye sensitized solar cells (DSSCs). The prospect of low-cost investments and fabrication are some of its key features. Today, with the development and intense research on the DSSC, there are records on devices with 13% efficiency, with high stability.[1] The increasing efforts to optimize DSSC devices establish a major challenge to the conventional solid-state photovoltaics technologies. While solid-state photovoltaics demands special laboratories to produce highly pure semiconductor materials, avoiding defects and interfaces, the DSSC, in contrast, is based on interface interactions (oxide/dye/electrolyte) and its preparation could be achieved in simple laboratory environment.

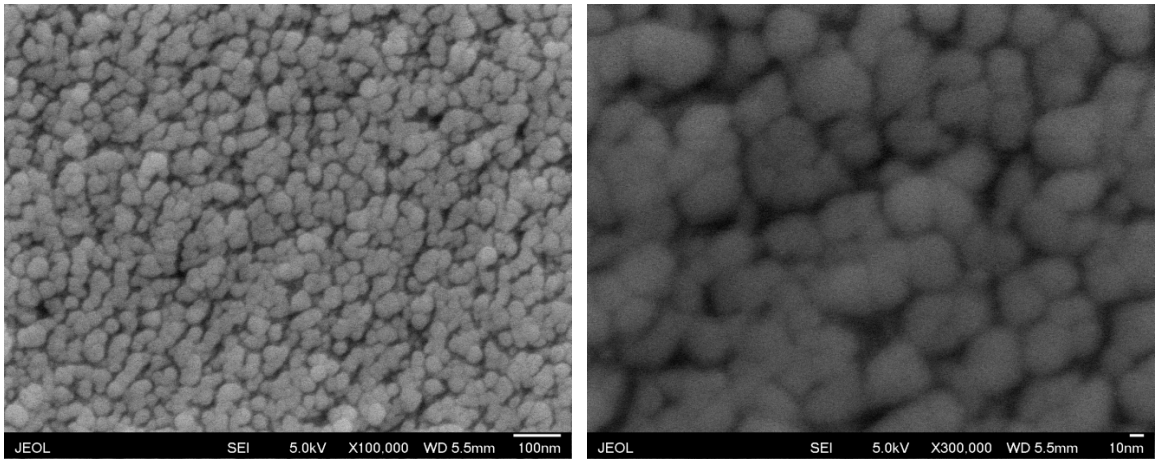

Figure II-1. Atomic Force Microscopy (AFM) of a mesoporous thin film of anatase TiO_2 nanoparticles. Mesoporous thin films are about 10 μm thick and each TiO_2 nanoparticle has approximately 20 nm diameter.[43]

The typical basic processes involved in a dye sensitized solar cell (DSSC) showing the principle of how the device operates are schematically depicted in Figure II-2, and can be found in many reviews in the area.[44, 102] At the heart of the device are the sintered TiO_2 nanoparticles (10 – 30 nm) interconnected in a mesoporous oxide thin layer (~10 μm and 50% porosity) to establish electronic conduction. The mesosporous thin layer is then deposited on a transparent substrate, which is commonly used the glass coated with fluorine-doped tin oxide (FTO). Anchored to the nanocrystalline film surface are the charge-transfer dye molecules working as sensitizers for light harvesting, see Figure II-3. Upon illumination, such sensitizers undergo to photogenerated excited states in a few femtoseconds resulting in ultrafast electron injection into TiO_2, on the subpicosencond time scale. After injection, the dye is left in its oxidized state due the loss of one electron. The sensitizer is regenerated to its ground state by electron transfer from the electrolyte, usually an organic solvent (commonly acetonitrile) containing the iodide/triiodide redox system. The regeneration step works on the microsecond domain, which effectively annihilates the oxidized dye molecules S^+ and intercepts the recapture (recombination) of the conduction band electrons with S^+, which happens in the millisecond time range. After I^- regenerates the oxidized dyes, the left I• radicals quickly reacts with others I^- ions to form the I_3^-. The formed triiodide ions diffuse through the electrolyte to the counter electrode, which is coated with a thin layer of platinum catalyst. Finally the regenerative cycle is completed when I_3^- is reduced back to I^- by electron transfer from the cathode.

Besides the desired electrons transfer process described above, there are undesired losses of energy through side reactions. Some of them are the direct relaxation of the dye excited state to its ground state defined by the excited state life time. Another major loss of energy in DSSC is the back reaction of the injected electrons in the TiO_2 with either oxidized dyes or acceptors redox mediator in the electrolyte. Figure II-2, depicts the general reaction processes in dye sensitized solar cells.

$S/TiO_2 + h\nu \rightarrow S^*/TiO_2$	Photoexcitation	(~fs)
$S^*/TiO_2 \rightarrow S^+/TiO_2 + TiO_2(e^-)$	Charge injection	(~ps)
$S^*/TiO_2 \rightarrow S/TiO_2 + h\nu' + \Delta$	Relaxation	(~ns)
$S^+/TiO_2 + I^- \rightarrow S/TiO_2 + I_3^-$	Regeneration	(~µs)
$S^+/TiO_2 + TiO_2(e^-) \rightarrow S/TiO_2$	Recombination	(~ms)
$TiO_2(e^-) + I_3^- \rightarrow I^-$	Regeneration	(~ms - s)

Figure II-2. Scheme of the possible reactions of charge transfer in a DSSC.

Energetic Features of the DSSCs

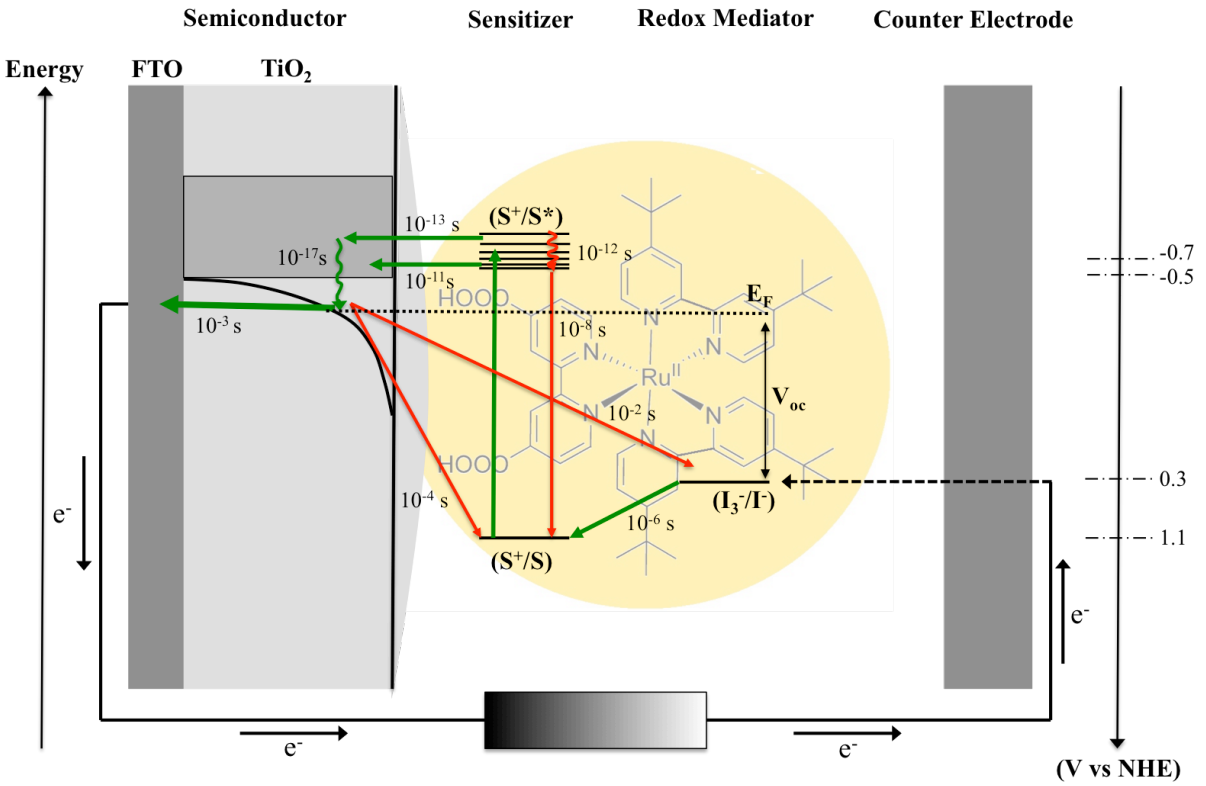

Figure II-3. Overview of processes and typical time constants under working conditions in a ruthenium-based dye solar cell with iodide/triiodide electrolyte. Recombination processes are indicated by red arrows.

Besides the attention to the limits in terms of kinetics, the energetics of DSSC is of fundamental importance to the function of the device, Figure II-3. This energetics comprises the positions of the energy levels at the oxide/dye/electrolyte interface, such as the energy levels for semiconductors, redox couples, and dye reduction potentials adsorbed to surfaces.

Before getting into details for the understanding of Figure II-3, it is necessary to make clear some important aspects of the concepts in energetics of the DSSCs. The diagram is a clear example of the interdisciplinarity created between physics and chemistry. While solid-sate physics normally uses the energy scale relative to the vacuum energy level, the electrochemistry has the potential scale with the standard hydrogen electrode (SCE) or the normal hydrogen electrode (NHE) as reference to the energy scale. For semiconductors, the electrochemical potential of electrons is commonly associated as the Fermi level, E_F, and systems in an electrolyte solution, it is normally referred to in potential as the redox potential, E_{redox}. The later basically represent the equilibrium potential where the concentrations of the redox states are equal. An estimated connection between the potentials of the NHE versus an electron in vacuum is given in Equation II-1.[103]

$$E_F[eV] = -4.5[eV] - eE_{redox}[V] \quad \text{(II-1)}$$

where *e* is the elementary charge. Most charge transfers in DSSC are limited to one electron reactions, which makes the conversion from Volts (V) to electronVolts (eV) straightforward.

For semiconductor, the equilibrium Fermi level is very sensitive to the environment and the determination of its absolute and relative energies in vacuum must be carefully analyzed in terms of their relevance to DSSC. Many electrochemical, photochemical, and spectroscopic studies have reported that mesoporous, nanocrystalline TiO_2 thin films possess several acceptor states tailing below the TiO_2 conduction band, E_{cb}, rather than an abrupt onset from an ideal E_{cb}.[43, 104] While there is emergent the belief that a well defined E_{cb} is not relevant to excited state injection it was found that the density of states (DOS) distribution at room temperature is of fundamental relevance to the functioning DSSC. At room temperature, this distribution is thought to have an exponential dependence on the applied voltage as determined from electrochemical[105-107] and spectroelectrochemical procedure[108]. The tail governed by an exponential dependence with the increase in energy arises from what is thought to be imperfections in the TiO_2 particle, where trapped states are energetically favorable to accept electrons.[43, 105, 109-110] The equilibrium Fermi level described by Boltzmann

statistics can be rearranged to isolate the cumulative number density of conduction band electrons at a specific energy, *E*.

$$n_c(E) = N_c \exp\left(\frac{E-E_c}{a \cdot k_B T}\right) \quad \text{(II-2)}$$

where N_c is the effective density of conduction band states, E_c is the energy at the conduction band edge, $k_B T$ is the thermal energy and a is the non-ideality factor. The non-ideality factor represents the deviation from the expected 59 mV increase in energy per decade of TiO_2 electron concentration.

Additionally, the non-exponential kinetics for excited-state electron injection can be rationalized supported by the exponential DOS at the TiO_2 surface.[111-114] And by assuming said distribution is composed of bulk, intra-bandgap states, diffusion of TiO_2 electrons, and dispersive recombination kinetics, the general kinetics for excite-state electron injection can be modeled satisfactorily by employing the continuous-time random walk model,[112, 115-119] which simulates the multiple-trapping detrapping events for charge recombination. The model is based on principles of dispersive transport where the waiting times for electrons motion are directly related to the energetics distribution of trap states.[117]

Besides the favorable kinetics for each charge transfer reaction, the energetics of the system is of fundamental importance. Dye molecules in its ground state have such positive potentials for oxidation that it would be impossible to initiate an electron transfer to the acceptor states of the TiO_2. However, when a sensitizer is photoexcited, it's more easily reduced or oxidized, because of the excitation free energy ΔG_{ES} stored in thexi state of the molecule. Electron injection will only occurs if the dye reduction potential at the excited state is above the distribution of TiO_2 acceptor states. Similarly, redox mediators, such as the I^-/I_3^- couple can only regenerate the oxidized dyes it can access the reduction potential of the sensitizer ground state.

The open circuit voltage, V_{oc}, represents the maximum energy that can be extracted from the system. It is the maximum Gibbs free energy that can be harnessed during steady state irradiance. The magnitude of V_{oc} is measured to be the difference between the quasi Fermi-level of the semiconductor and the redox couple, Figure II-3. Although the addition of cations, such as Li^+, in the electrolyte solutions aim to lower in energy the TiO_2 density of acceptor states to increase electron injection after photoexcitation, it is unfavorable to the V_{oc} once it would directly lower the energy of the quasi-Fermi level. The DSSC system

optimization in order to get higher V_{oc} values is a research field of major interest trying to find better redox mediator with more positive potentials and the molecular engineering trying to find dyes increasingly suitable for charge injection without the need of cations additions.

Photoinduced Electron Injection

DSSC have a unique feature when compared with other solar cell technologies, its charge separation state spatially separates the light absorber from the charge carrier transporter (for both electrons and holes), in other words, the two processes are independent and happen at different materials.

As previous discussed, the non-exponential kinetic for electron injection into TiO_2 is generally found to result from the heterogeneity of TiO_2, and its many consequences such as intra band-gap, trap states, electron diffusion into TiO_2, combined with the sensitizer binding modes and strengths, interactions between sensitizers and possible aggregates, and multiple ultrafast injection processes occurring from various states in the thermal relaxation pathway. The charge separation mechanism have been extensively studied in the past years, and it's believed injection can take place from multiple excited states in the thermal relaxation pathways with distinct rates.[38, 43, 120-121] More often, the injection pathways discussed are from the initially formed Franck-Condon singlet excited state (~ fs),[121] the thermally relaxed singlet excited state (~100 fs) and finally from the thermally relaxed triplet excited state after intersystem crossing from singlet excited state (~ ps).[38] The first and faster pathway is often called "hot injection" and is highly dependent on the excitation wavelength, TiO_2 Fermi level, and the distance between sensitizer and the semiconductor's surface. The slower component from triplet excited states in the picosecond regime results in biphasic injection kinetics.[122]

Extensively used in DSSCs, ruthenium based sensitizers like N3, N719 and black dye, have strong light absorption from and metal-to-ligand charge transfer (MLCT) state. The MLCT character promotes electrons, after excitation, from the metal center to the carboxylated bipyridyl ligand that is directly anchored to the semiconductor surface. In this fashion, excited-state charge separation occurs from the π^* orbitals of the organic ligand of the ruthenium complex to the acceptor states in TiO_2. The injection process for such ruthenium base dyes has been extensively debated. Ultrafast injection with time constants

>100 fs have been measured which would imply that injection is occurring before thermal relaxation of the molecular excited state.[43, 123] The slower component, in the picosecond range, is discussed as an injection mechanism proceeding via the lower energy triplet excited state. The spin-orbit coupling from the ruthenium heavy atom center enhances the probability for spin state changing and it gives the time for intersystem crossing to occur at hundreds of femtoseconds.[38]

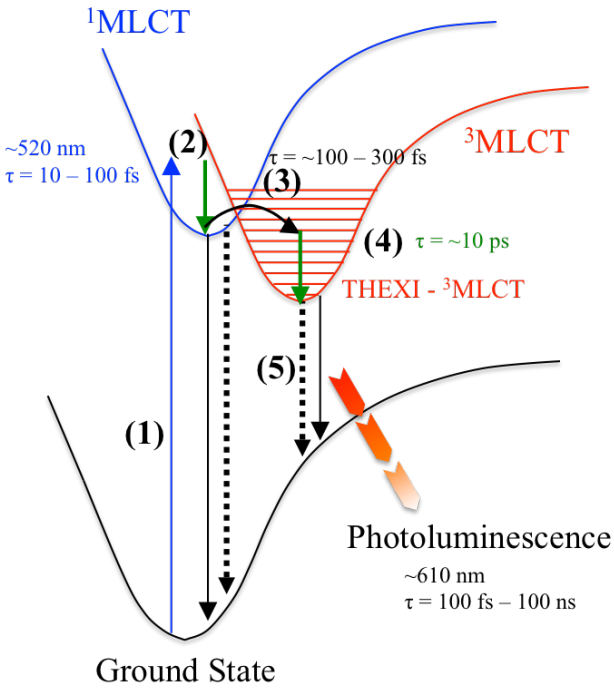

Figure II-4. Lennard-Jones potential energy diagram illustrating the relative electronic and vibrational energy and lifetime for a polypyridyl ruthenium(II) complex. Internal-conversion (2) and intersystem crossing (3) happens in the sub-picosecond time scale. The lifetime of the thermalized excited-state ranged on the nanosecond to microsecond time scale.

The theory for excited state electron injection into wide-bandgap semiconductor was first introduced by Gerischer.[36, 124-125] According to this theory, the rate of interfacial electron transfer at an electrode surface is proportional to the overlap of occupied electron donor with unoccupied acceptor states. Thus, in DSSCs, the rate constant and efficiency for electron injection critically depends on the overlap between the sensitizer excited-state distribution function and the semiconductor density of states (DOS).

$$k_{inj} \sim \int \kappa(E) D(E) W_{don}(E) dE \qquad \text{(II-3)}$$

where E is the energy, $\kappa(E)$ is the transfer frequency factor, $D(E)$ is the density of unoccupied acceptor states (DOS) in the semiconductor (electron acceptor), and $W_{don}(E)$ is the sensitizer donor distribution function (electron donor).

Regeneration of the Oxidized Dyes.

After photoinduced electron injection form the dye into the TiO_2 DOS, the dye is left in its oxidized state and an electron donor in the electrolyte for regeneration must reduce its ground state. In DSSCs, redox mediators are added to the external electrolyte. The reduced form of the mediator must regenerate the oxidized sensitizer by electron transfer prior to recombination with the injected electron. Then, the oxidized form of the redox mediator is reduced at the platinum counter electrode. Ideally, all redox states of the redox mediator would not competitively absorb light. By far the most effective donor in DSSCs is iodide.[126] In summary, the iodide/triiodide couple has good solubility, does not absorb too much light, has a suitable redox potential, and provides rapid dye regeneration. But, its major advantage is the very slow recombination kinetics between electrons in TiO_2 and the oxidized form of the redox mediator, the anionic triiodide (I_3^-), which could be associated with the electrostatic repulsion among the species.[127]

The regeneration of oxidized dyes with iodide leads to the formation of the diiodide radical ($I_2^-\bullet$),[128-131] observed for many groups using nanosecond transient absorption and pseudo-steady-state photoinduced absorption spectroscopy.[132] The pathway for dye regeneration by iodide is given by the reaction in Figure II-5.[43, 130, 133]

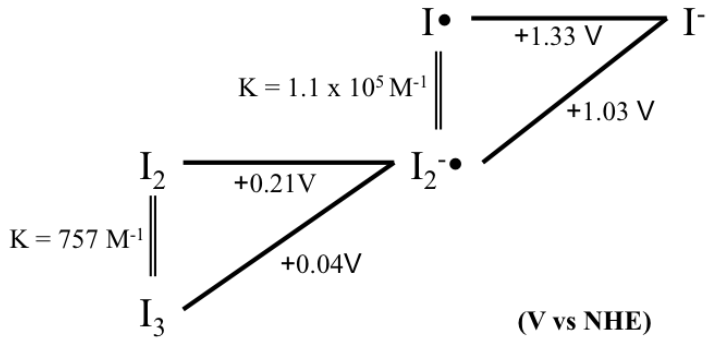

$S^* \rightarrow S^+ + TiO_2(e^-)$ (1)
$S^+ + I^- \rightarrow (S\cdots I)$ (2)
$(S\cdots I) + I^- \rightarrow (S\cdots I_2^-\bullet)$ (3)
$(S\cdots I_2^-\bullet) \rightarrow S + I_2^-\bullet$ (4)
$2I_2^-\bullet \rightarrow I_3^- + I^-$ (5)

Figure II-5. Scheme for the overall mechanism for sensitizer regeneration, where the I^-/I_3^- work as the redox mediator.

After electron injection from the excited dye S*, the oxidized dye S^+ is reduced by iodide, under the formation of the complex (S···I). The oxidation of iodide to free iodine radical (I•) is unlikely from energetic reasons: $E^0(I•/I^-)$ is +1.33 V vs NHE in aqueous solution,[134] and has been reported to +1.33 V vs NHE in acetonitrile,[135] which is more positive than the reduction potential, $E^0(S^+/S)$, for most of the dyes used as sensitizers in DSSCs. Unlikely, the redox potential of the iodine radical bound to the dye (S···I) is less positive in potential, so that its formation is expected to be the first step in the dye regeneration. The presence of a second iodide leads to the formation of ($S···I_2^-•$), which can dissociate into the regenerated dye at the ground state, S, and $I_2^-•$. Finally, $I_2^-•$ can disproportionate to produce triiodide and iodide. Nanosecond transient experiments have reported values for complete regeneration of the oxidized sensitizers on the microsecond scale, ~1 μs.[34, 37, 133, 136] The overall mechanism for the sensitizer regeneration is depicted in Figure II-5.

Charge Recombination: Energy Loss Mechanisms in the DSSC

A series of recombination reactions may harmfully compete with the desired reactions in the DSSC. Radiative and nonradiative decay from the thermalize photoexcited dye is a drain side reaction for electron injection. After photoinduced injection, electrons can undergo back reactions, recombination, with the oxidized sensitizers on the semiconductor surface. Moreover, injected electrons diffuse through the mesoporous TiO_2 nanocrystalline network before reaching and get collected by the conducting substract. Meanwhile, electrons may always be near the interface between TiO_2 surface and electrolyte becoming suitable to recombine with electron acceptors in the electrolyte. Because the V_{oc} is directly related with the electron concentration in the TiO_2 DOS undesired charge recombination processes the maximum Gibbs free energy that can be harnessed from the system can be compromised.

Quantitatively speaking, charge recombination with oxidized dyes have been widely studied over the last two decades, relative to the DSSC field.[34, 43, 116] Two models proposed by Nelson and Tachiya have been noteworthy for the observed charge recombination kinetics. The first one is established on the continuous-time random walk model (CTRW), where the transport of electrons is limited by a power law distribution of waiting time for electron

hoping between localized trapped states in the TiO_2 in a neighboring or nearby localized state.[34, 117] In this model, it was showed that recombination is limited by multiple trapping states of the $TiO_2(e^-)$ gives rise to stretched exponential decay, when trap states are exponentially distributed in energy.[116] Later, Tachyia *et al.* expanded the CTRW multiple-trapping model, proposed by Nelson *et al.*, to account for the possibility of many neighbor interactions, where electron can undergo multi-trapping and detrapping events through any available trap state in the nanoparticle as opposed to only nearest neighbors.[116-118]

Despite the difference in theory, both models reduce their decay kinetics to the stretched exponential Kohlraush-William-Watts (KWW) function. This function satisfactorily model the distribution of rate constants that were originated on the waiting time distribution of each trap-detrap event, predicted on the kinetics of the CTRW model.

$$A(t) = A_0 \, exp\left[-\left(\frac{t}{\tau_0}\right)^{\beta}\right] \tag{II-4}$$

where A_0 is the initial absorption change, τ_0 is the characteristic lifetime,[137] β is inversely related to the width of the underlying levy distribution of rate constants, $0 < \beta < 1$. The stretched exponential dispersion parameter β is related to the exponential distribution of trap states in the TiO_2, and also depends on the electrolyte composition[116] and the nature of the dye.[138] A mean lifetime for the kinetic process can be calculated from the first moment of the KWW function,

$$\langle\tau\rangle = \left(\frac{\tau_0}{\beta}\right)\Gamma\left(\frac{1}{\beta}\right) \tag{II-5}$$

where $\Gamma(x)$ is the Gamma function.[35, 82, 139]

It is noteworthy to say that not only electron recombination kinetics to oxidized dyes are well modeled to the KWW function, but likewise charge transfer recombination to the oxidized form of the redox mediator can be satisfactorily rationalized to the KWW stretched exponential function.[35, 43]

Ruthenium Polipyridyl Complexes in DSSC

Ruthenium(II) polypyridyl coordination compounds, among the metal complexes, have proven to show as most efficient sensitizers for solar harvesting and sensitization of wide-bangap TiO_2 semiconductor material,[43-44, 82, 111, 140-142] a consequence of their promising photovoltaic properties: a broad absorption spectrum, suitable excited and ground state energy levels, relatively long excited-state lifetime, and good electrochemical stability. The sensitization of the TiO_2 nanoparticles requires the Ru complexes to have functional groups, for anchoring activity, such as the carboxylic acid.[111, 143]

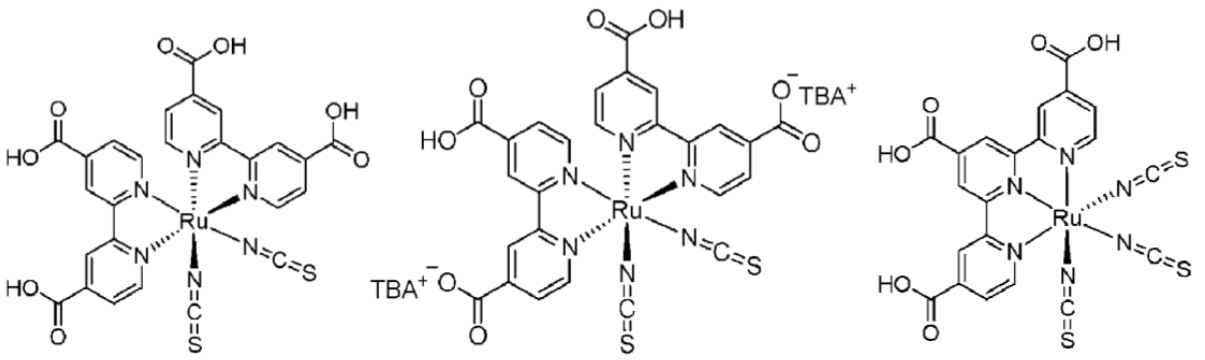

Figure II-6. Molecular structure of the ruthenium(II) based complexes used as sensitizers in DSSCs. Picture extracted from reference [44].[44]

In 1993, Grätzel and co-workers first introduced the *cis*-$(SCN)_2$bis(2,2′-bipyridyl-4,4′-dicarboxylate)ruthenium(II), better known as the N3 dye.[44, 144] It was revealed to have outstanding properties, such as broad absorption band in the UV-vis spectrum and photon-to-current conversion efficiency up to 800 nm, sufficiently long lived excited state (~20 ns), and strong adsorption on the TiO_2 surface. The N3 overall favorable properties granted it a solar-to-electric energy conversion efficiency of 10%, being the first time such efficiency is achieved for ruthenium(II) polypyridyl compounds.

Later, Nazeeruddin *et al.*[145] investigated the effect of protonation of the N3 dye anchoring groups on the performance of DSCs. The doubly protonated form, $(Bu_4N)_2[Ru(dcbpyH)_2(NCS)_2]$, coded N719, exhibited an improved power conversion

efficiency. The N3 and N719 dyes are considered as reference dyes for DSC and are used as a base for designing other Ru photosensitizers by changing ancillary ligands.

Seeking improvement in the efficiency of DSSCs, researches tried to extend the spectral light absorption of the sensitizer to the near-IR region, and many efforts have been made to change the ligands of the Ru complexes in order to accomplish such task. Therefore, Grätzel and co-workers designed the N749 dye, called the "black dye".[146] The study showed that the proposed molecular structure MLCT band red shifted due to the decrease in the π^* level of the terpyridine ligand and an increase in the energy of the metal orbital. The tuning to extend the light harvesting of the sensitizer led the achievement of photo-to-current conversion efficiency over the whole visible range covering into the near-IR region up to 920 nm and remarkable efficiency of 10.4%.[146]

Although ruthenium-based dyes are the most common sensitizers implemented in DSSCs, they have critical drawbacks. Ruthenium is not abundantly found in Earth, and it is unlikely the current supply will support the world energy needs if such ruthenium dyes DSSCs can be widely adopted for the realities of a solar-based economy. To overcome this challenge, extensive research has been done to substitute ruthenium sensitizers for inexpensive dye and easy to synthesize, while showing high efficiency.

Porphyrins as Sensitizers in DSSC

Porphyrins and phthalocyanines are widely known due to their primary role in photosysthesis and the ease with which their photophysical and photochemical properties can be tuned via molecular engineering. The use of porphyrins in DSSC was first introduced by Kay and Grätrzel in 1993,[10-11] and since that time the search for new efficient pophyrin dyes for DSSC have been strongly explored through molecular engineering. One of the disadvantages of ruthenium complexes is the limited absorption in the near-infrared region of the solar spectrum. Porphyrins and phthalocyanines exhibit intense spectral absorption bands in the near-IR region and possess good chemical, photo, and thermal stability, becoming potential candidates for sensitizers in DSSCs.

These porphyrins exhibit long-lived (>1 ns) π^* singlet excited states and depending on the central substituent, they show weak singlet/triplet mixing. They have an appropriate

LUMO level that resides above the conduction band of the TiO_2 and a HOMO level that lies below the redox couple in the electrolyte solution and very strong absorption of the Soret band in the 400-450 nm region, as well as the Q-band in the 500-700 nm region.[13, 15-16, 147-149] Several studies have demonstrated that porphyrin dyes can show efficient photoinduced electron injection into the conduction band of TiO_2[150-152] and that the oxidized state of the porphyrin dyes are mainly delocalized over the conjugated macrocycle ring.[151]

Based on the porphyrin structure there are two main points of attachment for TiO_2-binding groups, the *meso* and β positions, Figure II-7. DSSCs using porphyrins with *meso*-substituted benzoic acid binding groups (phenyl groups with carboxylic acid radical) are some of the earliest and still probably the most studied of the porphyrinoid-based sensitizers.[1, 149, 153]

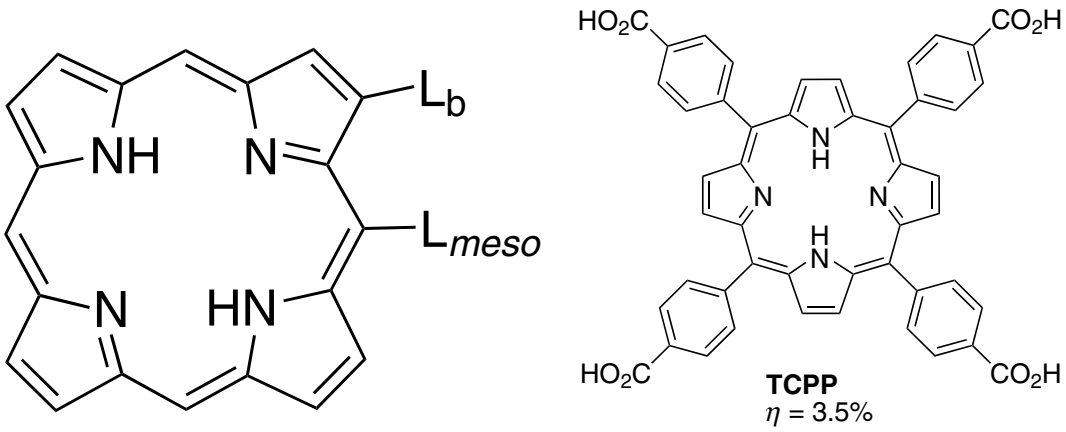

Figure II-7. On the left, it is shown the general structure for the free base porphryin ring with the two main points of attachment for TiO_2 binding groups, the *meso* positions (L_{meso}) and the β positions (L_b). On the right is the molecular structure the well known *meso*-substituted free base porphyrin with benzoic acid binding groups.

Although porphyrins have strong absorption in the UV and visible range of the electromagnetic spectrum, the absorptivity of this class of molecules as sensitizers in DSSCs is limited in the red an near infrared regions of the solar spectrum. Generally, *meso*-substituted porphryins have their outlying groups considered perpendicular to the plane of the macrocyclic ring and therefore are not in conjugation with the porphyrin π-conjugated system. To overcome such limitation, attempts to modify the *meso*-substituents by substitution at the macrocycle β-position with function groups have been widely employed to extend the π system to enhance the red-absorbing Q-bands.[154] The use of conjugated β-substituted

anchoring groups was first demonstrated in 2004 by Nazeeruddin *et al*. when they introduced a dye with an energy conversion efficiency of 4.1%.[155] Since then *β*-substituted porphyrins have achieved efficiencies greater than 7% and have been synthesized to study substituent effects.[154, 156]

Although it was proved that modification of the *β*-position of porphyrin is an effective strategy to optimize the energy levels and improve the efficiency of DSSCs, porphyrin dyes have shown lower photovoltage compared with Ru sensitizers.[157] One major cause may be due to a significantly reduced electron lifetime in porphyrin-based DSSCs. In related DSSCs, the zinc porphyrins gave a better performance in comparison with the corresponding free-base dyads.[158] Probably because zinc-porphyrins have longer S_2 excited state lifetimes that is favorable for hot-injection from higher energy excited states.[27] Also, the presence of metal ions in the porphyrin center effectively changes the macrocycle photophysical and photochemical properties, which favors the efficiency for charge separation at the interface and the overall cell efficiency. In 2014, Grätzel *et al*. have reported a new record on DSSCs efficiency of 13% after using molecular engineering to tune the desired sensitizer's properties on a zinc-porphyrin.[1]

CHAPTER 3: Adsorption of a Free-Base Porphyrin *meso*-substituted with Ruthenium(II) groups, $H_2TPyP[Ru(bpy)_2NO_2]_4$, on Mesoporous TiO_2 Thin Films, in the Absence of Functional Binding Groups.

3.1. INTRODUCTION

The work done during the first 2 years of the current DSc proposal was basically centered on the photophysical properties and characterization of porphyrin compounds. A wide variety of techniques were employed to accomplish such task, for instance steady state spectroscopy (UV-vis absorption and photoluminescence), time-resolved spectroscopy (excited state lifetime and transient absorption) and excited state non-linearity. In 2013 the opportunity to join in the governmental program Science without Borders (Ciência sem Fronteiras – CsF) as an exchange visiting student in the USA was fulfilled in an outstanding research laboratory led by Prof. Gerald J. Meyer, in the Johns Hopkins University (JHU), Baltimore – MD, USA. In addition to improve the knowledge in the photophysical and photochemical research field as well as the learning of new experimental techniques, the major focus of research at Meyer's groups covers one of the world most highlighted research topics: the solar energy conversion to energy – the solar cells – and more specifically, the dye sensitized solar cells (DSSC), considered to be the potential candidates for the future of solar energy conversion.

In this fashion, the research work line proposed as a visiting student at JHU would involve porphyrins obtained from collaborative networks of Prof. Newton Barbosa Neto with a synthesis specialized group from Prof. Alzir Batista in the Departamento de Química, Universidade Federal de São Carlos (UFScar), São Carlos – SP, Brazil. The said collaboration was established in the past given the seriousness that Prof. Newton leads his research. A

group of porphyrin ruthenium-base complexes were selected to the following work in Meyer's laboratories with the possibility to employ them as sensitizers in DSSC.

The current PART II of this dissertation, composed by Chapter 3, tries to create a coherent "bridge" between what was done prior to the experience at JHU, and what ended up being the convergence to a possible new research line adopted by Prof. Newton group – the observation of photodriven charge and energy transfer in organic and inorganic system. While PART I remains focused in the analysis of porphyrin systems, PART III is completely devoted to phenomena of processes enclosed in DSSC systems. The sudden deviation will be satisfactorily discussed in this chapter.

The current section of this dissertation is focused on a new free base tetrapyridyl porphryin *meso*-substituted with a ruthenium complex, $Ru(dmb)_2NO_2$, Figure 3.1. The said molecule, although absent of functional binding groups, was suitable for sensitization of TiO_2 through what is believed to be electrostatic interactions with the nanocrystallite surface. The porphyrin extensively discussed in Chapter 2 has also been tested for TiO_2 sensitization, but the attachment was very inefficient, certainly because of the absence of binding groups.

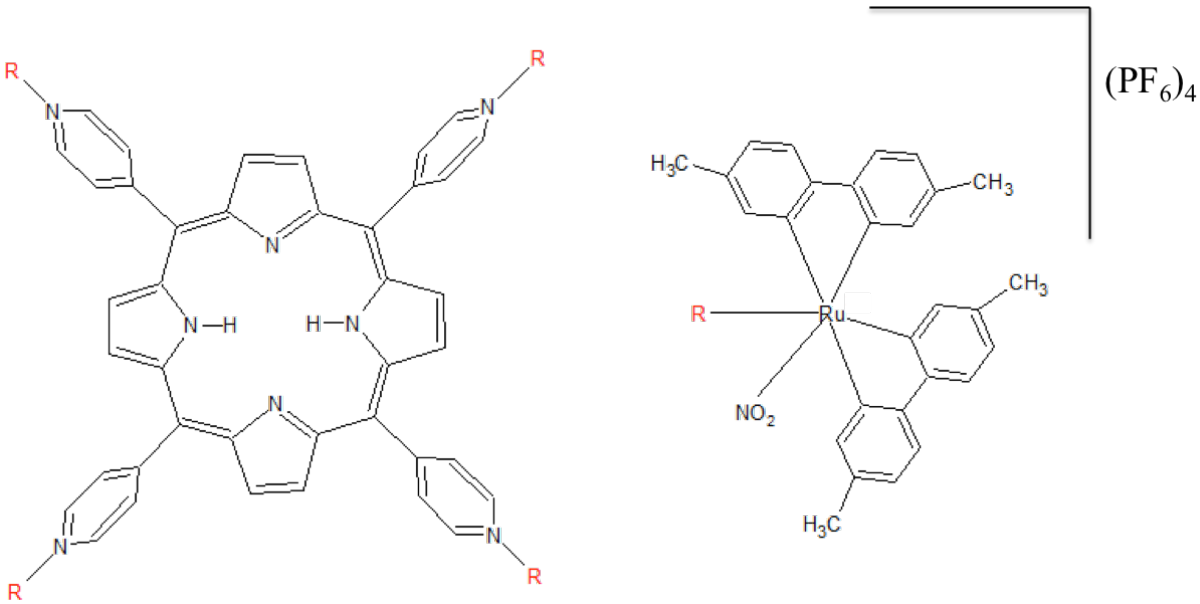

Figure 3.1. Molecular structures of $\{H_2TPyP[Ru(dmb)_2NO_2]_4\}(PF_6)_4$, where R = $[Ru(dmb)_2NO_2]PF_6$. Here (dmb) stands for 4,4′-Dimethyl-2,2′-dipyridyl.

For reasons discussed above, the only attempt to studied porphyrin complexes adsorbed onto TiO_2 surfaces was done for the H_2TPyP-$RuNO_2$.

3.2. EXPERIMENTAL METHODS

3.2.1 – Materials and Preparations

Materials. The following reagents were used as received from the indicated commercial suppliers: acetonitrile (CH_3CN; Burdick & Jackson, spectrophotometric grade); lithium perchlorate ($LiClO_4$; Sigma-Aldrich 99.99%); Rhodamine B (Sigma Aldrich, ≥95.0%); argon gas (Airgas, >99.998%); and glass microscope slides (Fisher Scientific, 1mm thick).

Preparation. The ruthenium and porphyrin compounds were synthesized by the group of Prof. Alzir Batista from the Departamento de Química of the Universidade Federal de São Carlos.

Transparent TiO_2 nanocrystallites (anatase, ~15 nm in diameter) were prepared by acid hydrolysis of Ti(*i*-OPr)$_4$ using a sol-gel method previously described in the literature.[143] The sols were cast as transparent mesoporous thin films by doctor blading onto glass microscope slides for spectroscopic measurements and transparent FTO conductive substrates for electrochemical measurements with the aid of transparent cellophane tape as a mask and spacer (~10 μm thick). The films were sintered at 450 ºC for 30 minutes under an atmosphere of O_2 flow and either used immediately or stored in an oven for future use. Sensitization was achieved by immersing the thin films in acetonitrile sensitizer solutions (mM concentrations) for hours to days depending on the desired surface coverage.

3.2.2 – Spectroscopy

UV-Vis Absorption. Steady-state UV-visible absorption spectra were obtained on a Varian Cary 50 spectrophotometer at room temperature in 1.0 cm path length quartz cuvette. The solutions were prepared with known concentration, from which was obtained their extinction coefficient, ε, using Beer-Lambert's Law. For further studies of photoluminescence and transient absorption the solutions were purged with argon gas for a minimum of 20 minutes. Sensitized TiO_2 thin films were positioned at a 45º angle in cuvettes filled with the indicated acetonitrile solutions. The solutions were purged with argon gas for a minimum of 30 min prior to transient absorption and spectroelectrochemical studies.

Photoluminescence. Steady-state photoluminescence (PL) spectra and excitation spectra (ES) were obtained with a Spex Fluorolog spectrophotometer equipped with a 450 W Xe lamp for the excitation source, with samples dissolved in acetonitrile, argon gas purged, and placed in a 1.0 cm thick quartz cell. Was used a 90^o configuration for detection of the signal. The excitation wavelengths were adjusted using a monochromator placed between the light source and the sample. The concentration employed in these optical measurements were controlled via absorption measurements such that the absorption at the excitation wavelength did not exceed 0.2, in order to avoid reabsorption effects.

Photoluminescence quantum yield was calculated using the actinometry method where Rhodamine B was the reference standard.

Transient absorption. Nanosecond transient absorption measurements were obtained with an apparatus similar to that which has been previously described in the literature.[82] Briefly, samples were excited by a Q-switched, pulsed Nd:YAG laser (Quantel U.S.A. (BigSky) Brilliant B; 5−6 ns full width at half-maximum (fwhm), 1 Hz, ~10 mm in diameter) tuned to 532 nm with the appropriate nonlinear optics. The excitation energy was measured by a thermopile power meter (Molectron) and was typically 1−5 mJ/pulse so that the absorbed energy was typically <1 mJ/pulse. A 150 W xenon arc lamp served as the probe beam and was aligned orthogonal to the laser excitation light. The lamp was pulsed with 100 V for detection at sub-100 μs time scales. Detection was achieved with a monochromator (Spex 1702/04) optically coupled to an R928 photomultiplier tube (Hamamatsu). Appropriate glass filters were positioned between the probe lamp/sample and the sample/detection monochromator. Transient data was acquired with a computer-interfaced digital oscilloscope (LeCroy 9450, Dual 350 MHz) with an overall instrument response time of ~10 ns. Typically, 30 laser pulses were averaged at each observation wavelength over the range 400−750 nm, at 3 or 5 nm intervals. Full spectra were generated by averaging 2−10 points on either side of the desired time value to reduce noise in the raw data. For single wavelength measurements, 90−180 laser pulses were typically averaged to achieve satisfactory signal-to-noise ratios.

3.3. RESULTS AND DISCUSSIONS

3.3.1 – Steady State Experiments and the Electrostatic Interaction with TiO_2.

The electronic spectra of the porphyrin H_2TPyP-$RuNO_2$ and the adsorbed H_2TPyP-$RuNO_2/TiO_2$ are present in Figure 3.2A. The H_2TPyP-$RuNO_2$ UV-Vis absorption spectrum presented strong peaks at the UV spectral region, where the well-known singlet high energy transition, the Soret band was found at 417 nm, with ε = 162,000 M^{-1} cm^{-1}. Regarding to the Q bands, the characteristic D_{2h} symmetry of the porphyrin reflects their splitted four-banded absorption spectrum in the Q-band region,[84] localized at 516 nm, 552 nm, 590 nm and 646 nm.

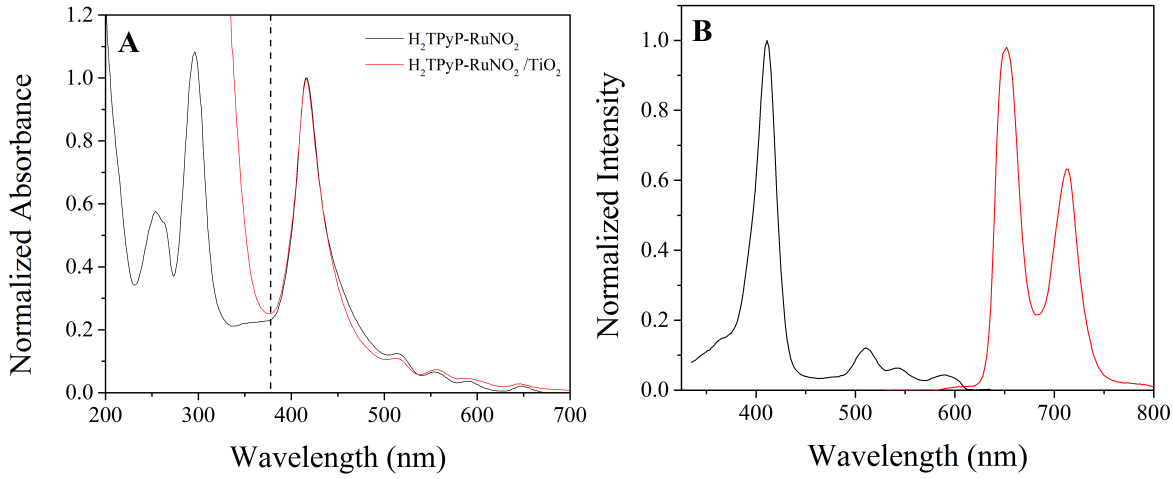

Figure 3.2. (A) Steady-state UV-Vis absorbance spectra of H_2TPyP-$RuNO_2$ in acetonitrile solution (black) and the electrostatically attached compound to the TiO_2 surface, H_2TPyP-$RuNO_2/TiO_2$ (red). The black dotted line separates the absorption range from the dye to the fundamental absorbance of the TiO_2. (B) Normalized steady state excitation spectrum, probed at 650 nm, (black) and photoluminescence spectrum, excited at 532 nm, (red) of H_2TPyP-$RuNO_2$ in acetonitrile solution.

Similarly to what was observed in Chapter 2, when compared to the H_2TPyP, the H_2TPyP-$RuNO_2$ shows intense absorption band in the ultraviolet spectral range ascribed to intraligand $\pi \rightarrow \pi^*$ transitions within the (dmb) ligands. The activation of new vibrational modes after the complexation of H_2TPyP with the $Ru(dmb)_2NO_2$ triggered the broadening and

the decrease in oscillator strength of the Soret band. The ruthenium groups did not significantly perturbed the porphyrin lowest singlet excited state, S_1, maintaining the *phyllo* type for the Q bands relative intensity, which is supported by the excitation spectrum, Figure 3.2B. The metal-to-ligand charge transfer (MLCT) of the $Ru(dmb)_2NO_2$ is overlapped with the porphyrin Soret band. Sensitization achieved through electrostatically adsorbing the porphyrin dyes on the TiO_2 surface led to negligible changes in the UV-vis absorption spectral shape, Figure 3.2A.

PL experiments on H_2TPyP-$RuNO_2$ exhibited very similar photoluminescence spectral features with the unsubstituted H_2TPyP,[13] with peaks at 650 nm and 711 nm. Photoluminescence quantum yield calculation found 0.06%, value expressing efficient excited state quenching mechanisms through non-radiative relaxation processes back to the ground state.

The conclusions proposed in Chapter 2 are very similar to what was observed in preliminary spectroscopic studies on the H_2TPyP-$RuNO_2$ porphryin.

3.3.2 – Transient Absorption and the Possibility of Electron Injection.

Solution transient absorption experiments on H_2TPyP-$RuNO_2$, probed at 470 nm, have revealed the existence of an exponential relaxation process, yielding lifetimes of 130 μs (40%) and 12 μs (60%), Figure 3.3A. Porphyrin with peripheral ruthenium groups have shown to be very sensitive in their triplet excited states. Usually, the observed trend is the porphyrin-ruthenium compound having a much larger triplet excited state life time when compared to the porphyrin without the ruthenium groups (0.6 μs). This behavior was better observed and discussed in Chapter 2.[13-15, 71, 75] Although there exist two different lifetimes to the transient state disappearance, it still remain unknown the real source to address such processes.

Once was obtained a high surface coverage for H_2TPyP-$RuNO_2$ sensitized TiO_2 thin films, transient absorption experiments were found to be suitable to investigate whether charge injection could appear in such system. The transient absorption spectrum of a free base tetrapyridyl porphyrin shows a characteristic bleach of the ground state between 400 nm and 430 nm, and a growth from 430 nm to 500 nm. The results showed clear similarity in the transient absorption spectral shape of H_2TPyP. Besides the Soret band bleach, other small

bleaches to longer wavelengths of the transient absorption spectrum revealed the structuration of the Q bands. The pronounced growth starting at 650 nm could be immediately misunderstood as $TiO_2(e^-)$ in the conduction band, if the certainty of electron injection is not proven to be the case. Moreover when adsorbed on the TiO_2 surface, the transient kinetic trace of H_2TPyP-$RuNO_2$, did not accept bi-exponential adjustments. Instead, the adjustment to the KWW fitting function combined with a bi-exponential function revealed the presence of a fast deactivation process.

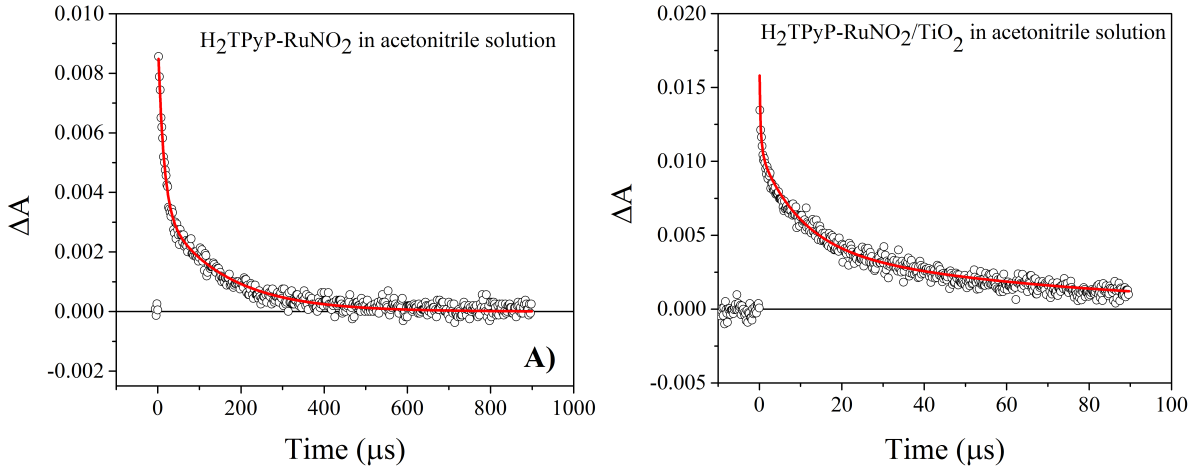

Figure 3.3. Single wavelength kinetics (470 nm) transient absorption of H_2TPyP-$RuNO_2$: (A) in acetonitrile solution; and (B) adsorbed on the TiO_2 surface immersed in neat acetonitrile.

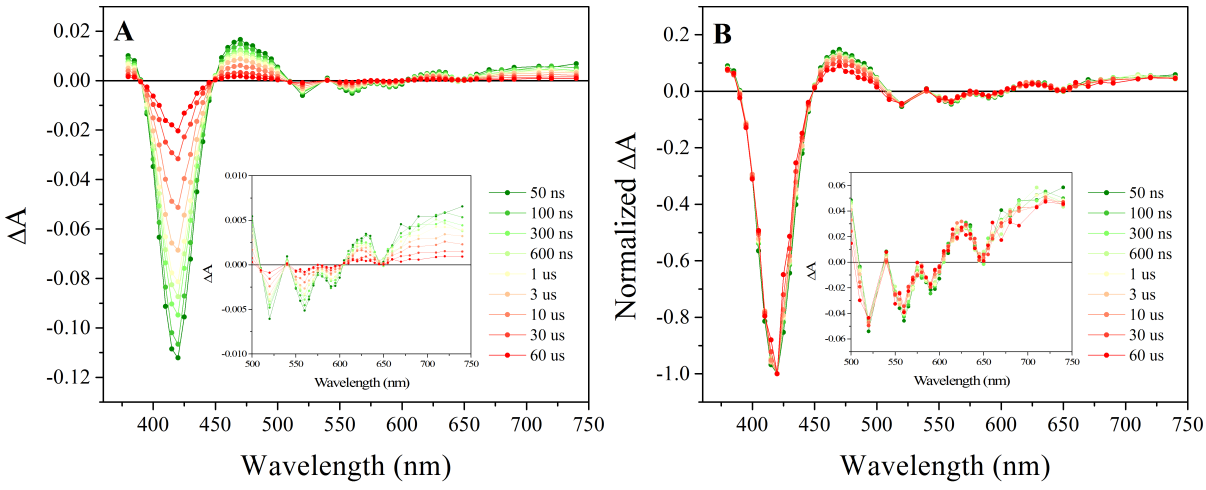

Figure 3.4. (A) Transient absorption spectra after pulsed 532 nm excitation of H_2TPyP-$RuNO_2/TiO_2$ in neat acetonitrile. (B) Its normalized representation. The inset figures show the rescaled transient spectra from 500 nm to 750 nm for better visualization.

The found fitting parameters are: 270 ns (44%), 10 µs (33%), and 70 µs (23%). Many porphyrins used in DSSCs are known to have lower cell efficiencies due to fast electron recombination processes, so that the observed fast component responsible for 44% of the ΔA signal could be associated to the back electron transfer from the TiO_2 to the oxidized porphyrin. Although speculative, such results reinforce the necessity to perform photoelectric experiments to make sure whether current can be generated by the sensitization of H_2TPyP-$RuNO_2$ in TiO_2 thin films.

The potential energy diagram for electron transfer process showed a favorable driving force for electron transfer from the ruthenium peripheral groups to the porphyrin ring, Figure 3.5. Although transient absorption experiments are able to address many electron transfer processes, in this case would be necessary to perform spectroelectrochemical experiments to better understand the oxidized and reduced forms of the absorbance spectrum of the porphyrin compound. So that by comparison with the photogenerated transient absorption spectrum, it would be possible to satisfactorily address specifics changes in absorbance spectrum to electron transfer processes.

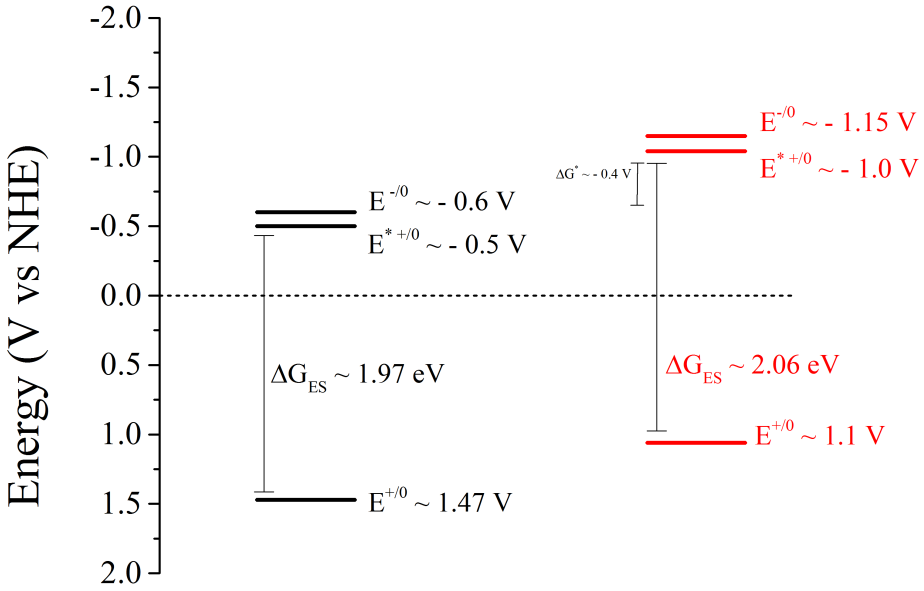

Figure 3.5. Reduction potential diagram for electron transfer processes of H_2TPyP- $RuNO_2$. The black lines are potentials associated with the porphyrin ring while the red lines are the potentials for the $RuNO_2$ moiety, in acetonitrile.

3.4. CONCLUSIONS

The attempts to sensitize TiO_2 nanoparticle with porphyrins for charge transfer studies were found to be unpromising. Chapter 2 gives an overall possible explanation for the unsatisfactory mechanism. In brief, complexation of substituted free base porphyrin with peripheral ruthenium groups in the porphyrin ring *meso*-position mainly interact with higher energy excited states from the π-conjugated system of porphyrins which are known to have very fast lifetime (~fs), while the long lived S_1 states do not overlap with the ruthenium complex orbital for possible intermolecular charge transfer. Also, the absence of functional binding groups does not create stable adsorption of the porphyrin on the semiconductor surface, moreover the presence binding groups, such as the carboxylic acid (COOH), gives the moiety an electron withdrawing characteristic which is favorable to charge transfer. Photoelectron injection could be present in transient absorption experiment, however to truly precise this information, photoelectric experiments (*e.g.* incident photon-to-current efficiency – IPCE) should be performed.

The initially proposed work plan of porphyrin studies as possible dye sensitizers for DSSCs was found to be worthless due its strong limitations. However very good insights and finding were of fundamental importance for a better understand on the working mechanism of DSSC and the necessity of molecular engineering to tune porphyrin photophysical and photochemical properties.

With the failure of the initial proposal, alternative works had to be initiated. The fact that Prof. Meyer's laboratory was specialized in ruthenium polypyridyl complexes, and not such proximity with porphyrin synthesis, was the first step in the research line changing. The fundamental purpose when working in Prof. Meyer's laboratory was to learn the overall science that rules the working mechanism of the DSSCs. In this fashion, adjust the possibilities to the needs was an inherent act.

The research focused on the ruthenium-based dyes started through the understanding of the photophysics and photochemistry of such inorganic coordination groups. Latter, I was introduced to a very interesting effect found in DSSCs that happens right after electron injection, called the Stark effect. In summary, such effect is the perturbation of the photophysical and photochemical properties of the anchored dyes caused by the presence of a surface electric field originated from the photoinduced injected electrons. The Stark effect in

DSSCs has recently being a target of exaustly research as the presence of a surface electric field might be relevant to the overall working mechanism of the dye sensitized solar cells.

PART III:

Stark Effect in Mesoporous TiO_2 Thin Films Sensitized With Pyridine Based Ruthenium Compounds.

INTRODUCTION

An Introduction to the Stark Effect and its Implications to the Dye Sensitized Solar Cells

Johannes Stark observed splittings of the hydrogen atom induced by an electric field nearly 100 years ago,[159-160] and his name has been associated with this class of effects ever since. Measurements of Stark splittings of spectral lines in the gas phase continue to this day, both to obtain fundamental properties of states and transitions and as a diagnostic tool in complex systems such as plasmas. Stark spectroscopy is less widely applied in condensed phases, as large electric fields are needed to detect the effect for inhomogeneously broadened lines.[160-161]

In a molecular level understanding, an external electric field applied to a molecule will cause a reorganization of its electron distribution, resulting in a change in the Hellmann-Feynman force acting on the constituent nuclei. The field also exerts a force directly on the nuclei. The resulting net force will induce changes in molecular geometry, vibrational and electronic properties.[162]

The evolution of the Stark effect concept and its potential use as a tool to understand molecular properties has been attractive, for many years, to the research community. A particular research area, created ever since, of attractive interesting and remarkable importance is the application of the Stark effect in spectroscopy to experimentally determine the change in dipole moment, $\Delta\mu$, and polarizability, $\Delta\alpha$, for a transition in molecular systems. This research area was then named the Stark Spectroscopy.[161, 163]

In the conventional Stark spectroscopy, application of an external electric field to molecules that are immobilized and not oriented, *e.g.* in a glass or polymer film, leads to the broadening, shifts and change in intensity of the electronic absorption spectra, due to changes in dipole moment, $\Delta\mu$, polarizability, $\Delta\alpha$, and oscillator strength, respectively. The contributions of each type of electro-optic property can be extracted by comparing the observed change in absorption in the field with the second, first and zeroth derivatives of the absorption spectrum, respectively. For an isolated absorption band in a non-oriented, immobilized sample where the shift of the transition energy upon application of an electric

field $\vec{E}$, $\Delta\nu$ (usually expressed in units of cm^{-1}), is smaller than the inhomogeneous bandwidth, the change in absorption upon application of an external field is given by: [161, 163]

$$\Delta A(\nu) = E^2 \left\{ A_\chi A(\nu) + \frac{B_\chi}{15hc} \nu \frac{d}{d\nu} \left(\frac{A(\nu)}{\nu} \right) + \frac{C_\chi}{30h^2c^2} \nu \frac{d^2}{d\nu^2} \left(\frac{A(\nu)}{\nu} \right) \right\} \quad \text{(III-1)}$$

A better description of Equation III-1 can be found in references [161] and [163]. But briefly, decomposition of the ΔA spectrum for an isotropic immobilized sample into absorption derivative components yields values for A_χ, B_χ and C_χ which then can be used to extract information on the molecular parameters: transition moment ($\vec{m}$), polarizability ($\Delta\alpha$) and change in dipole moment ($\Delta\vec{\mu}$).

In the simplest physical terms, Equation III-1 can be better understood as following. The random orientations of $\Delta\vec{\mu}$ relative to the applied field direction lead to a spread in the transition energy; the difference between this broadened lineshape and the lineshape in the absence of a field is just the second derivative of the absorption. The molecular polarizability change, $\Delta\alpha$, interacts with the field to induce a dipole moment typically in the direction of the field. Because this field-induced dipole moment is oriented with respect to the field, the spectrum shifts either to higher or to lower energy, depending on the sign of $\Delta\alpha$; this lineshape is the first derivative of the absorption spectrum.[163]

Many molecules, especially those asymmetric characterized by electron donating and withdrawing groups, exhibit strong dipole moments in both ground and excited state, as consequence of the distribution of electron density across the molecule. Dipole moments are defined to point from the negative charge (δ−) to the positive charge (δ+). Some molecules may have, in their ground state, an intrinsic distribution of charges which leads to the appearance of a ground state dipole moment, ($\vec{\mu}_G$). When In their excited state, molecules usually undergo charge transfer processes between its molecular orbitals generating a new charge density configuration, leading to a dipole moment in the excited state ($\vec{\mu}_{ES}$). The preferential directions of each dipole moment, ($\vec{\mu}_G$) or ($\vec{\mu}_{ES}$), is highly dependent on the properties of the molecules with their electron donor-acceptor moieties interactions. The change in dipole moment upon excitation ($\Delta\vec{\mu}$) is defined as:

$$\Delta\vec{\mu} = \vec{\mu}_{ES} - \vec{\mu}_G \quad \text{(III-2)}$$

This quantity gives information about the magnitude of the intramolecular charge

transfer upon excitation and is therefore an important parameter in the characterization dye molecules, especially for Stark effect experiments.

An electric field applied to a molecule will cause a reorganization of the electron distribution, such that the resulting net force is responsible for noticeable induced effects: changes in the intensity of electronic and vibrational transitions bands, shifts in their frequencies and degeneracy splitting.[164]

In very general terms the change in transition energy (ΔU) due to an external electric field ($\vec{E}$) is given by,

$$\Delta U = -\Delta\vec{\mu} \cdot \vec{E} - \frac{1}{2}\vec{E} \cdot \Delta\alpha \cdot \vec{E} \qquad \text{(III-3)}$$

where is evident the presence of a first order Stark effect, which is linear in the electric field, and the second order Stark effect , which is quadratic in the electric field. Cappel *et al* have extensively worked with the Stark spectroscopy on organic dyes used in dye sensitized solar cells and they found that changes in the transition absorption spectrum were linear with the electric field,[165] so that Equation (III-3) can be reduced to $\Delta U = -\Delta\vec{\mu} \cdot \vec{E}$. Also in this work, Cappel *et al* have proposed that the contribution of the Stark Effect, under the limitation to small perturbation approximation, could be well modeled by the first derivate of the ground-state spectrum, given by a relation that accounts for the spectral shift of wavenumbers $\Delta\nu$, in cm^{-1}, of the transition related to a change in dipole moment, $\Delta\vec{\mu}$, under the presence of an electric field $\vec{E}$.[165-166]

$$\Delta A = \frac{dA}{d\tilde{\nu}}\Delta\nu = \frac{dA}{d\nu}\left(\frac{-\Delta\vec{\mu}\cdot\vec{E}}{ch}\right) \qquad \text{(III-4)}$$

Considering dye-sensitized solar cells, there is a crescent search for understandings of how the Stark effect affects electronic transitions of dye molecules adsorbed to titanium dioxide surfaces. In this case, the perturbation of an electric field is originated from electrons that were injected, from a molecular excited state, into the TiO_2 nanoparticles right after light absorption. As the dye molecules are adsorbed onto the nanoparticle surface and the electric field is emanated from its surface, it is convenient to define a main direction of the electric field, which is normal to the titanium dioxide surface. On average, dye molecules adsorbed to the surface should therefore experience an almost uniform electric field in one direction, so

that the relation $\Delta U = -\Delta\vec{\mu} \cdot \vec{E}$ rewritten in a one-dimensional form (which can be chosen to be along the normal vector to the TiO_2 nanoparticle):

$$\Delta U = -\Delta\mu \cdot E \qquad \text{(III-5)}$$

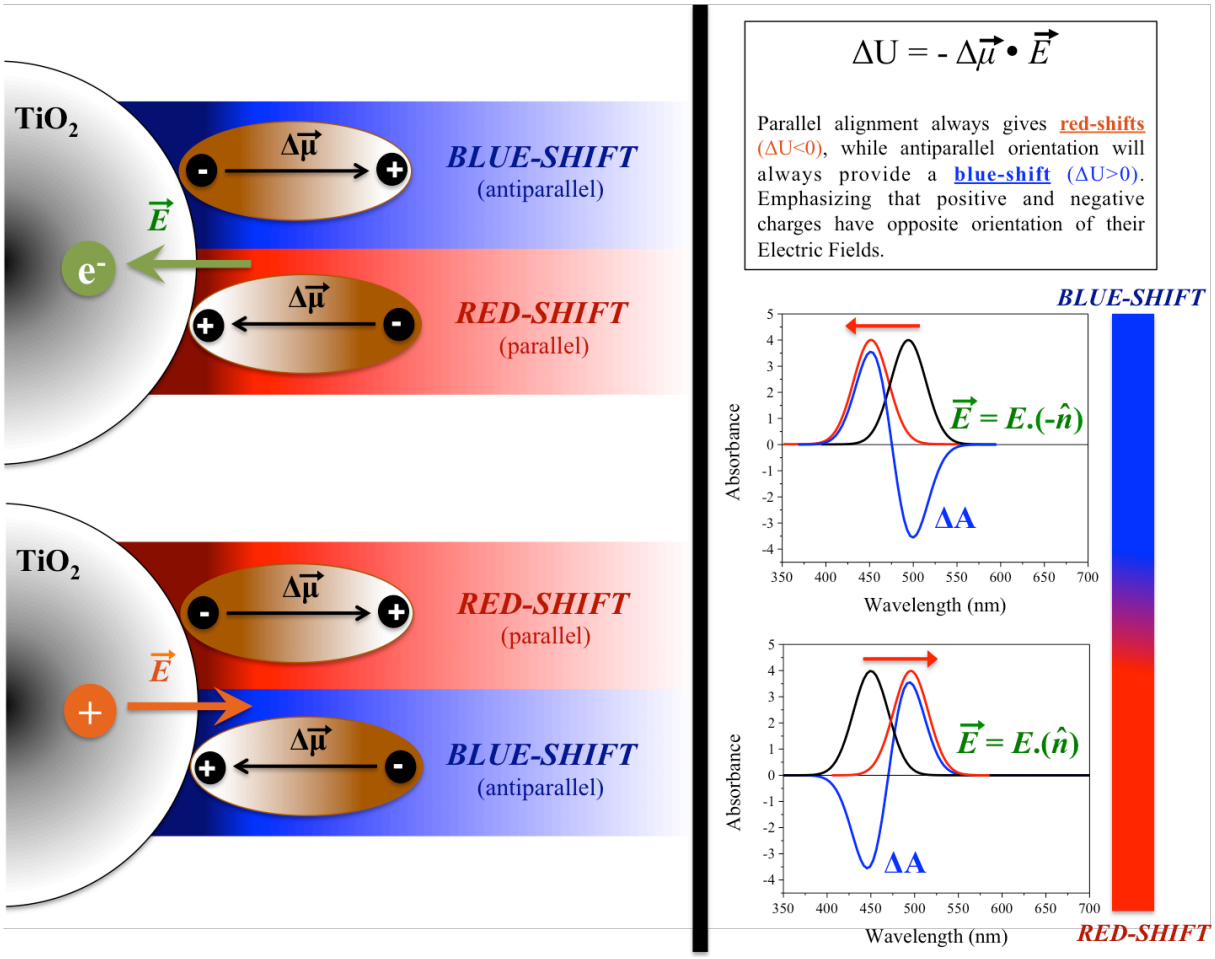

Figure III-1. Electric field direction outside the TiO_2 nanoparticle in which point charges are presented inside the TiO_2. On the right is shown the first order Stark shift in both cases, when $\boldsymbol{\Delta\vec{\mu}}$ is parallel and antiparallel to the electric field $\vec{\boldsymbol{E}}$. The gaussians in black represent the initial conditions of a random absorption transition while those in red are the perturbed transitions by an external electric field resulting in frequency shifts. The quantity $\boldsymbol{\Delta A}$ is the difference spectrum $\boldsymbol{\Delta A = A_{final} - A_{initial}}$.

The scheme shown in Figure III-1, summarizes the possible alignments configurations between the change in dipole moment and the surface electric field leading to the resultant frequency shift of the molecular transitions.

Traditional electroabsorption analysis, through the classical Stark Spectroscopy, predicts that a change in dipole moment, $\Delta\vec{\mu}$, would give rise to a second-derivative spectrum rather than the first-derivative. [161, 163, 167-168] When electron are injected into the TiO_2 nanoparticles, its electric field is emanated preferentially normal to the TiO_2 surface, while the overall orientation of sensitizers remains unchanged. This makes the field orientation with respect to each sensitizer's lowest energy change in dipole moment always predominantly in a collinear configuration, resulting in an unidirectional shift of the absorption spectrum, which resembles its first derivative spectrum.[169]

Most of the Transient Absorption employed in the study of dye sensitized solar cells end up on the following equation:

$$\Delta A = \Delta A_{Oxidized} + \Delta A_{ES} + \Delta A_{electrons} + \Delta A_{Stark} \quad \text{(III-6)}$$

where ΔA express the difference in absorbance between an initial state, where molecules are presented in its ground state, and a final state which might be composed by oxidized molecules, excited state, the presence of electrons in the TiO_2 conduction band, and the shifted ground state absorbance, so that it generates $\Delta A_{Oxidized}$, ΔA_{ES}, $\Delta A_{electrons}$, and ΔA_{Stark}, respectively.

The injected electron in TiO_2 nanoparticle leaves behind an oxidized dye, which is regenerated on the nanosecond time scale by the redox chemistry of I^-/I_3^-. The excited state for the molecule under study has its life time around 300 nanoseconds in neat acetonitrile and is substantially quenched by the addition of cations in the electrolyte. With this in mind, within a secure time window starting after the first 1μs, the Equation III-6 can be reduced to:

$$\Delta A = \Delta A_{electrons} + \Delta A_{Stark} \quad \text{(III-7)}$$

As the electron extinction coefficient at the UV-Vis spectral frame is considerably small, showing reasonable evidence of its existence only at the red spectral region, the major observed ΔA within the UV-Vis spectral frame is specifically attributed to the Stark Effect.

In this dissertation work, the Stark effect was observed in two different types of measurements: 1) in Spectroelectrochemical experiments in which electrochemically accumulation of electron in the density of states of the TiO_2 nanoparticles is achieved by the application of negative potentials; and 2) in Transient Absorption Experiments, which the

electric field is induced after photoinjection from the excited state dye molecules adsorbed on the TiO_2 surface.

In Chapter 4, is proposed the analysis of a heteroleptic ruthenium complex adsorbed on TiO_2 thin films that have its absorption spectrum perturbed by electric fields from either electrochemically accumulation of electrons or injected electrons right after pulsed laser excitation. The Stark effect is systematically studied as a function of four different types of cations adsorbed on the TiO_2 surface: Na^+, Li^+, Mg^{2+} and Ca^{2+}. The nature of each cations critically defines the strength of the electric field ant the TiO_2 – dye molecule interface based on screening mechanisms.

While in Chapter 4, the Stark effect is observed in the presence of metal ions salts of perchlorates and the redox mediator I^-/I_3^-, Chapter 5 gives an approach in which a ruthenium compound composed by a mono-pyridine ligand is absorbed to the TiO_2 surface. The ruthenium complex showed efficient electron injection in the absence of adsorbed cation and excited state formation wasn't observed under the experimental conditions used. Under such conditions, the observed ΔA in transient spectroscopy was composed exclusively by $\Delta A = \Delta A_{Oxidized} + \Delta A_{electrons} + \Delta A_{Stark}$. It was possible to probe the Stark effect in neat solvent, acetonitrile, in transient absorption experiments. Critical insights, which concerns about charge motion and screening the high TiO_2 permittivity, were satisfactorily obtained. Finally, Chapter 5 proposes a new model to report the time evolution of the Stark effect, under restrict conditions.

CHAPTER 4 – Electric Fields and Charge Screening in Dye Sensitized Mesoporous Nanocrystalline TiO_2 Thin Films.

4.1. INTRODUCTION

The 1991 Nature paper by Grätzel and O'Regan introduced the clever idea of utilizing mesoporous thin films of nanocrystalline TiO_2 in photoelectrochemical cells[170]. The idea turned out to be revolutionary and created whole new fields of science based on energy conversion with nanometer-sized semiconductor materials.[171-172] The nanometer length scale can result in very different photoelectrochemical behavior than that observed in bulk semiconductor materials. For example, in single crystal and thin films materials, electron-hole pairs are efficiently separated by a surface electric field (the 'depletion' or 'space charge' region) that is absent in weakly doped semiconductor nanocrystallites.[173] In fact, the three bias conditions identified for single crystal semiconductor materials, i.e. depletion, inversion, and accumulation, are not particularly useful for quantifying or modeling the photoelectrochemistry of semiconductor nanocrystallites. In the case of dye-sensitized solar cells (DSSCs), it has generally been assumed that any electric fields that might be present under illumination would be completely screened from the surface anchored dye molecules by the large dielectric constant of TiO_2, $\varepsilon_r = 7 - 50$;[174] the high permittivity of acetonitrile, $\varepsilon_r = 37$;[175] and the half molar ionic strength of the electrolyte.

The assumption of quantitative charge screening at sensitized TiO_2 interfaces was proven to be incorrect in 2010, when two groups reported that electrons injected into TiO_2 had a profound influence on the absorption spectrum of dye molecules anchored to the surface.[165, 176] The absorption changes measured after the injection of charge were similar to those previously reported in traditional Stark spectroscopic measurements,[167-168, 177-178] but were unidirectional due to the fixed orientation of the molecular dipole moment relative to the TiO_2 surface. With some assumptions, the spectral shifts reported directly on the magnitude of the electric field that was found to be substantial, on the order of 2.7 MV/cm.[176] It remains

unclear whether this electric field or charge screening is relevant to power conversion in DSSCs. The spectral shift of the dye molecules is generally small and does not appreciably change the light harvesting efficiency of the sensitized thin film. Likewise, the potential drop experienced by the dye molecules represents a fairly small value of ~ 40 mV that corresponds to only about 5% of the open circuit photovoltages reported for gold standard DSSCs.[176] In fact, charge screening may have a deleterious influence on energy conversion efficiencies with anionic redox mediators like I^-/I_3^-. Synonymous to increasing the width of the space-charge layer in bulk semiconductor solar cells, increasing the Debye length for charge screening at the semiconductor electrolyte interface should aid in the generation of even further spatially separated and longer-lived anionic charges, *i.e.* $TiO_2(e^-)$s and I_3^-, and hence improve solar conversion efficiencies. While speculative, fundamental studies of surface electric fields and charge screening may provide new insights into the fabrication of superior DSSCs. Such studies are also of intellectual interest in their own right.

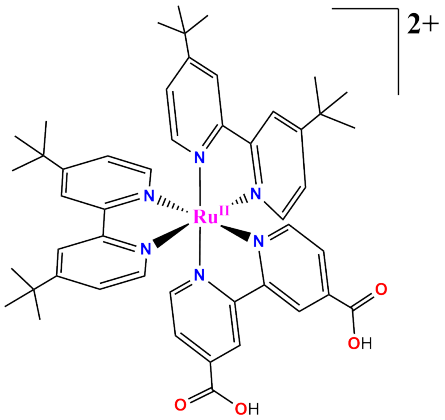

Figure 4.1. The structure of $Ru(dtb)_2(dcb)^{2+}$.

An intriguing observation from previous research was that following pulsed laser excitation of sensitized TiO_2 thin films immersed in an acetonitrile electrolyte, the magnitude of the Stark effect decreased over time periods in which the $TiO_2(e^-)$ concentration was constant.[176] This behavior was attributed to the reorganization of interfacial ions and solvent molecules responding to the electrons that were photoinjected into TiO_2, a process often referred to as "screening". While screening of this type is well known in the electrochemical and photo-electrochemical literature,[179-184] to our knowledge this represents the first opportunity to probe the dynamics of this process on short time scales. The kinetics for charge screening were reported to be sensitive to whether Mg^{2+} or Li^+ cations were present in the electrolyte.[185] The study of $[Ru(dtb)_2(dcb)](PF_6)_2$, where dtb is 4,4′-(*tert*-butyl)$_2$-2,2′-

bipyridine and dcb is 4,4′-$(CO_2H)_2$-2,2′-bipyridine, was utilized as the compound is a particularly sensitive probe of the surface electric field Figure 4.1. Here these studies were expanded to include Na^+ and Ca^{2+}. The inclusion of these ions influenced the screening dynamics as well as the interfacial density of states and the excited state injection yield.

4.2. EXPERIMENTAL METHODS

4.2.1 – Materials and Preparations

Materials. The following reagents and substrates were used as received from the indicated commercial suppliers: acetonitrile (CH_3CN; Burdick & Jackson, spectrophotometric grade); deionized water; lithium perchlorate ($LiClO_4$; Sigma-Aldrich 99.99%); sodium perchlorate ($NaClO_4$; Sigma-Aldrich, 99%); magnesium perchlorate ($Mg(ClO_4)_2$; Sigma-Aldrich, ACS Reagent); calcium perchlorate tetrahydrate ($Ca(ClO_4)_2 \cdot 4H_2O$; Sigma-Aldrich, 99%); tetra-*n*-butylammonium perchlorate ($TBAClO_4$; Aldrich, ≥99.0%); tetra-*n*-butylammonium iodide (TBAI; Fluka, ≥99.0%); argon gas (Airgas, >99.998%); oxygen gas (Airgas, industrial grade); titanium(IV) isopropoxide (Sigma-Aldrich, 97%); fluorine-doped SnO_2-coated glass (FTO; Hartford Glass Co., Inc., 2.3 mm thick, 15Ω/□); and glass microscope slides (Fisher Scientific, 1mm thick). $[Ru(dtb)_2(dcb)](PF_6)_2$ was available from previous studies.[176]

Preparations. Transparent TiO_2 nanocrystallites (anatase, ~15 nm in diameter) were prepared by acid hydrolysis of Ti(*i*-OPr)$_4$ using a sol-gel method previously described in the literature.[143] The sols were cast as transparent mesoporous thin films by doctor blading onto glass microscope slides for spectroscopic measurements and transparent FTO conductive substrates for electrochemical measurements with the aid of transparent cellophane tape as a mask and spacer (~10 μm thick). The films were sintered at 450 ºC for 30 minutes under an atmosphere of O_2 flow and either used immediately or stored in an oven for future use. Sensitization was achieved by immersing the thin films in acetonitrile sensitizer solutions (mM concentrations) for hours to days depending on the desired surface coverage. Unless otherwise noted, the thin films were sensitized to roughly maximum surface coverage, $\Gamma \sim 7 \times 10^{-8}$ mol/cm^2, which was determined using a modified Beer—Lambert law,[186]

$$Abs = 1000 \times \Gamma \times \varepsilon \quad (4.1)$$

where ε is the molar decadic extinction (absorption) coefficient (16,400 $M^{-1}cm^{-1}$ at 465 nm) that was assumed to have the same value when anchored to the surface. Sensitized films were soaked in neat acetonitrile for at least one hour prior to experimentation.

4.2.2 – Spectroscopy and Electrochemistry

UV-Visible Absorption. Steady-state UV-Visible absorption spectra were obtained on a Varian Cary 50 or an Agilent Cary 60 spectrophotometer at room temperature in 1.0 cm path length quartz cuvettes. Sensitized TiO_2 thin films were positioned at a 45º angle in cuvettes filled with the indicated acetonitrile solutions. The solutions were purged with argon gas for a minimum of 30 min prior to transient absorption and spectroelectrochemical studies.

Photoluminescence. Steady-state photoluminescence (PL) spectra were obtained with a Spex Fluorolog spectrophotometer equipped with a 450 W Xe lamp for the excitation source. PL spectra of sensitized thin films were obtained under ambient conditions at room temperature with excitation 45º to the surface and detection from the front face of the sample. Quenching experiments were performed by obtaining the PL spectrum of the sensitized thin film in neat solvent and after replacement of the neat solvent with the electrolyte solution of interest.

Transient Absorption. Nanosecond transient absorption measurements were obtained with an apparatus similar to that which has been previously described in the literature.[82] Briefly, samples were excited by a Q-switched, pulsed Nd:YAG laser (Quantel USA (BigSky) Brilliant B; 5-6 ns full width at half-maximum (fwhm), 1 Hz, ~10 mm in diameter) tuned to 532 nm with the appropriate nonlinear optics. The excitation fluence was measured by a thermopile power meter (Molectron) and was typically 1-5 mJ/pulse so that the absorbed fluence was typically <1 mJ/pulse. A 150 W xenon arc lamp served as the probe beam and was aligned orthogonal to the laser excitation light. The lamp was pulsed with 100 V for detection at sub-100 microsecond time scales. Detection was achieved with a monochromator (Spex 1702/04) optically coupled to an R928 photomultiplier tube (Hamamatsu). Appropriate glass filters were positioned between the probe lamp/sample and the sample/detection monochromator. Transient data was acquired with a computer-interfaced digital oscilloscope (LeCroy 9450, Dual 350 MHz) with an overall instrument response time of ~10 ns. Typically,

30 laser pulses were averaged at each observation wavelength over the range 400 – 750 nm, at 3 or 5 nm intervals. Full spectra were generated by averaging 2-10 points on either side of the desired time value to reduce noise in the raw data. For single wavelength measurements, 90-180 laser pulses were typically averaged to achieve satisfactory signal-to-noise ratios. Relative excited-state electron injection yields were measured by comparative actinometry on the nanosecond time scale for samples in different metal cation solutions using lithium as the reference.[142, 187]

Electrochemistry. A potentiostat (Bioanalytical Scientific Instruments, Inc. (BAS) model CV-50W or EC Epsilon electrochemical analyzer) was employed for electrochemical measurements in a standard three-electrode arrangement with a TiO_2 thin film working electrode, a Pt gauze counter electrode (BAS), and a non-aqueous silver reference electrode (BAS). The ferrocenium/ferrocene ($Fc^{+/0}$) half-wave potential was measured both before and after experiments in a 100 mM $TBAClO_4$/acetonitrile electrolyte that was used as an external standard to calibrate the reference electrode. All potentials are reported versus the normal hydrogen electrode (NHE) through the use of a conversion constant of -630 mV from NHE to $Fc^{+/0}$ in acetonitrile at 25 ºC.[188]

Spectroelectrochemistry was conducted via simultaneous application of an applied potential while monitoring the UV-Vis absorption spectra of TiO_2 thin-film electrodes in the indicated electrolytes. Each applied potential was held for 2-3 min, until the absorbance in the 700-900 nm region became invariant in time. Single-wavelength absorption features plotted as a function of the applied potential were proportional to the cumulative formation/loss of states; for the $TiO_2(e^-)$ absorption features, this was directly related to the cumulative TiO_2 density of acceptor states.[189]

Spectroelectrochemical charge extraction measurements were performed on un-sensitized TiO_2 thin films to obtain the extinction coefficient of the $TiO_2(e^-)$s. In these experiments, the absorbance at 700 nm was recorded as the potential was stepped from +200 mV to increasingly negative values. The charge present in the film was measured coulometrically after stepping the potential back to the original +200 mV value. [190-192] The absorption values were corrected for the 45º angle of the thin film in relation to the optical path. Each charge extraction cycle was repeated 3 times at each applied bias.

4.3. RESULTS AND DISCUSSIONS

Thin films of TiO_2 on glass substrates were reacted with $Ru(dtb)_2(dcb)^{2+}$, abbreviated $Ru(dtb)_2(dcb)/TiO_2$, in acetonitrile solutions to a maximum surface coverage, $\Gamma \sim 7 \times 10^{-8}$ M^{-1} cm^2.[176] Representative absorption spectra of $Ru(dtb)_2(dcb)/TiO_2$ immersed in neat acetonitrile and 100 mM perchlorate acetonitrile solutions are shown in Figure 4.2A. The $Ru(dtb)_2(dcb)/TiO_2$ samples exhibit a metal-to-ligand charge transfer (MLCT) absorption band centered at 465 nm in neat acetonitrile and the fundamental TiO_2 absorption below 380 nm. The spectrum measured in neat acetonitrile and in 100 mM $TBAClO_4$ (where TBA is tetra-*n*-butylammonium) were within experimental error the same. Replacement of the neat acetonitrile solvent bath with 100 mM metal perchlorate salt acetonitrile electrolytes resulted in a bathochromic shift, the magnitude of which was dependent on the cation. The MLCT absorption shifts to ~480 nm for monovalent cations, Li^+ and Na^+, and to ~486 nm for divalent cations, Mg^{2+} and Ca^{2+}, shown in Figure 4.2A.

Visible light excitation of the MLCT absorption band resulted in room temperature photoluminescence (PL), shown in Figure 4.2B. In neat acetonitrile, $Ru(dtb)_2(dcb)/TiO_2$ exhibited a PL maximum at 665 nm. Upon replacement of the neat solvent with 100 mM metal perchlorate electrolytes: the PL maximum red-shifted and the PL intensity was quenched to varying extents dependent on the nature of the cation. The corresponding quantities are compiled in Table 4.1.

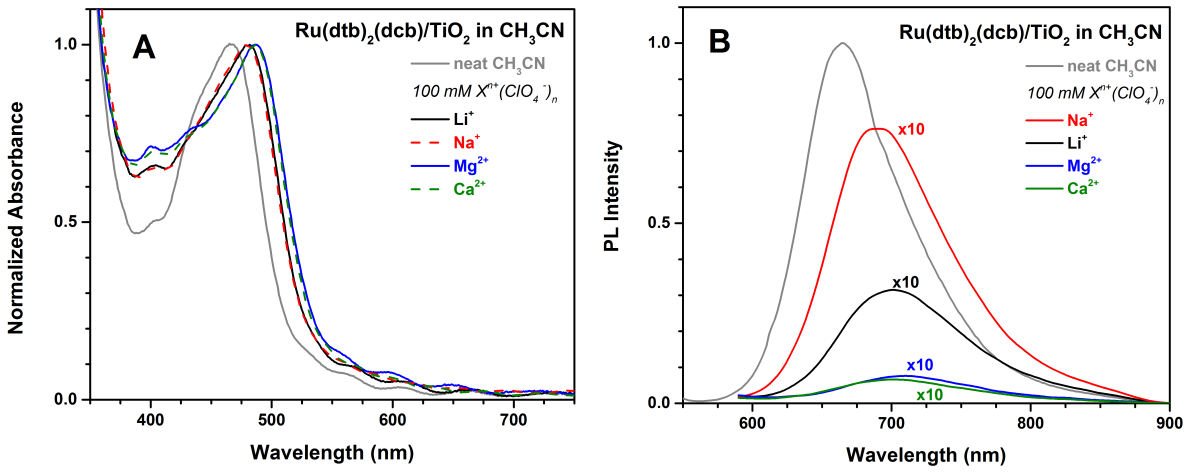

Figure 4.2. Steady-state UV-Vis absorbance (A) and photoluminescence (B) spectra of $Ru(dtb)_2(dcb)/TiO_2$ in neat acetonitrile and in the presence of 100 mM metal perchlorate electrolyte.

Table 4.1. Photophysical and electrochemical properties of $Ru(dtb)_2(dcb)/TiO_2$ in 100 mM metal perchlorate acetonitrile solutions.

Cation	Abs_{max} (nm)[a]	PL_{max} (nm)	ΔG_{es} (eV)[b]	$E^0(Ru^{III/II})$ (V vs. NHE) and (α)[c]	$E^0(Ru^{III/II*})$ (V vs. NHE)[d]
neat CH_3CN	465	665	2.05	---	---
Li^+	480	700	1.86	1.46 (1.39)	-0.40
Na^+	480	690	1.88	1.43 (1.35)	-0.45
Mg^{2+}	486	710	1.88	1.49 (1.58)	-0.39
Ca^{2+}	486	700	1.90	1.50 (1.74)	-0.40

[a]Wavelengths are ±1 nm. [b]The free energy stored in the excited state. [c]The $Ru^{III/II}$ reduction potential and the ideality factor, α. [d]The excited state reduction potential calculated using Equation 3.

Electrochemical reduction of un-sensitized TiO_2 thin films resulted in a blue shift of the fundamental absorption and the appearance of a broad absorption in the visible region. When measured as difference spectra, the blue shift of the fundamental absorption appears as a bleach, the magnitude of which was sensitive to the identity of the cation, Figure A4.1 in the Appendix. Charge extraction experiments were performed on un-sensitized TiO_2 thin films to determine the molar extinction coefficients of the $TiO_2(e^-)$ absorption band in each of the four metal perchlorate electrolytes. The absorption at 700 nm was monitored while the applied potential was stepped from 200 mV to -400 mV vs. NHE for 65 s and then returned to the initial 200 mV potential, Figure A4.2 in the Appendix. The absorption was corrected for the 45º angle of the thin film relative to the optical path. Plotting the corrected absorbance versus the extracted charge from the film at multiple potentials allowed for determination of the molar extinction coefficient from the slope of a linear fit to the data, shown in Figure A4.3 in the Appendix. The extinction coefficient was independent of the electrolyte composition within experimental error and was determined to be $\varepsilon(TiO_2(e^-)) = 930 \pm 50\ M^{-1}\ cm^{-1}$ at 700 nm. The application of more negative potentials, i.e. < -1.2 V, resulted in new absorption features that were not studied in detail due to the irreversible nature of the absorption changes, Figure A4.4 in the Appendix.

In order to understand the ground-state behavior, spectroelectrochemistry was performed on sensitized TiO_2 thin films in 100 mM metal perchlorate acetonitrile electrolytes. Application of a positive applied potential resulted in spectral changes consistent with the oxidation of Ru^{II} to Ru^{III}, shown in Figure A4.5 in the Appendix. The equilibrium potential

where the concentration of Ru^{II} and Ru^{III} were equal was taken as the $E^o(Ru^{III/II})$ reduction potential for $Ru(dtb)_2(dcb)/TiO_2$. The spectroelectrochemical data were fit to Equation 4.2:

$$x = \frac{1}{1+10\exp\left(\frac{E_{app}-E^0}{\alpha \times 59\ mV}\right)} \tag{4.2}$$

where x is the fraction of molecules in each oxidation state, E_{app} is the applied potential, and α is the ideality factor. Knowledge of $E^o(Ru^{III/II})$ allowed for the estimation of the reducing power of the excited state which was calculated through a free energy cycle using Equation 4.3:

$$E^0\left(Ru^{III/II*}\right) = E^0\left(Ru^{III/II}\right) - \Delta G_{ES} \tag{4.3}$$

where ΔG_{ES} is the Gibbs free energy stored in the MLCT excited state determined by a tangent line extrapolation back to zero intensity on the high energy side of the PL spectrum. The formal reduction potentials and ideality factors are summarized in Table 4.1.

Application of a forward (negative) bias resulted in reduction of TiO_2 that was monitored by the characteristic broad absorption features from 400 to 900 nm attributed to $TiO_2(e^-)$s. Concomitant with the $TiO_2(e^-)$ absorption, the MLCT absorption band blue-shifted. Both of these spectral features are evident in Figure 4.3 for a $Ru(dtb)_2(dcb)/TiO_2$ thin film in 100 mM $LiClO_4$ acetonitrile solution with an applied bias ranging from 150 to -750 mV vs. NHE. The normalized spectroelectrochemical absorption spectra are shown in Figure 4.3A and after subtraction of the contributions from $TiO_2(e^-)$s in Figure 4.2B. Difference spectra of these same data are shown in Figure 4.3C and D.

The electric field experienced by the surface-bound sensitizers as a function of the applied potential bias was calculated using both peak-to-peak and first-derivative analysis methods and are compared in the insets of Figure 4.3A and B. For the peak-to-peak analysis, the electric field was calculated using Equation 4.4:

$$\Delta\upsilon = -\frac{|\Delta\vec{\mu}|\cdot|\vec{E}|\cdot\cos\theta}{100hc} \tag{4.4}$$

where h is Planck's constant, c is the speed of light in a vacuum, $\Delta\upsilon$ is the change in spectroscopic peak maximum (in wavenumbers), $\Delta\vec{\mu}$ is the change in dipole moment vector

between the ground and excited state, $\vec{E}$ is the electric field vector, and θ is the angle between the latter two quantities. With the assumption of $\theta = 180°$ and $\Delta\vec{\mu} = 4.75$ D,[167, 193] the electric field can be calculated at each applied bias. Similarly, the first-derivative analysis was performed using Equation 4.5:

$$\Delta A = -\frac{dA}{d\nu}\frac{\Delta\vec{\mu}\vec{E}}{h} \tag{4.5}$$

where ΔA is the difference spectrum, or delta absorbance, and $\frac{dA}{d\nu}$ is the first derivative of the absorbance spectrum (in wavenumbers).[165] The electric field calculated using both the peak-to-peak analysis and the first-derivative analysis were in good agreement, as seen in the insets of Figure 4.3A and B.

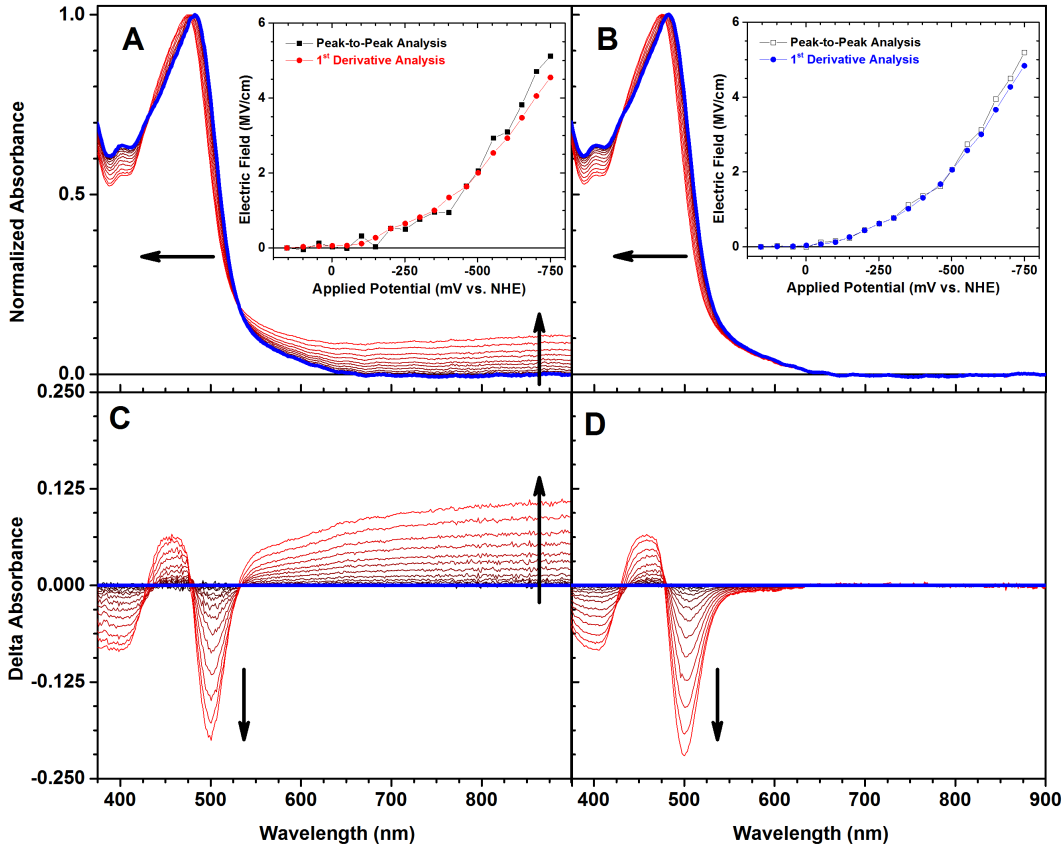

Figure 4.3. Spectra of a potentiostatically controlled $Ru(dtb)_2(dcb)/TiO_2$ film in 100 mM $LiClO_4$ acetonitrile solution (A); and after subtraction of the long-wavelength $TiO_2(e^-)$ absorption (B). The difference spectra for the data shown in A and B are given in C and D, respectively. The insets in A and B indicate the electric field strength calculated by two different analyses. The spectra in dark blue were recorded at +150 mV and spectra recorded at more negative potentials (up to -750 mV) are indicated in red. The arrows indicate the direction of change with increased negative applied potential.

The electric field experienced by the surface-bound sensitizers was calculated using the electron corrected spectra and the first-derivative method for all four cations and is shown in Figure 4.4 as a function of the applied potential (A) and the estimated electron concentration per TiO_2 nanoparticle (B). The latter was calculated by converting the applied potential to the number of $TiO_2(e^-)$s per 15 nm diameter particle through the measured absorbance and Beer's law using the measured extinction coefficient and the effective optical path length for a 10 μm thick film of 50% porosity.[194] For example, in 100 mM metal ion perchlorate solution where ε = 930 cm^{-1}, an absorbance of 0.0124 would correspond to 20 $TiO_2(e^-)$s/particle with Equation 4.6:

$$Abs = \varepsilon \times l \times c(TiO_2(e^-)) = 930\ (M^{-1}cm^{-1}) \times 14.14 \times 10^{-4}\ (cm) \times 50\% \times \frac{(TiO_2(e^-))}{{}^4/_3\pi(7.5\times10^{-9}\ (m))^3 \times N_A \times 10^3 (L\ m^{-3})} \quad (4.6)$$

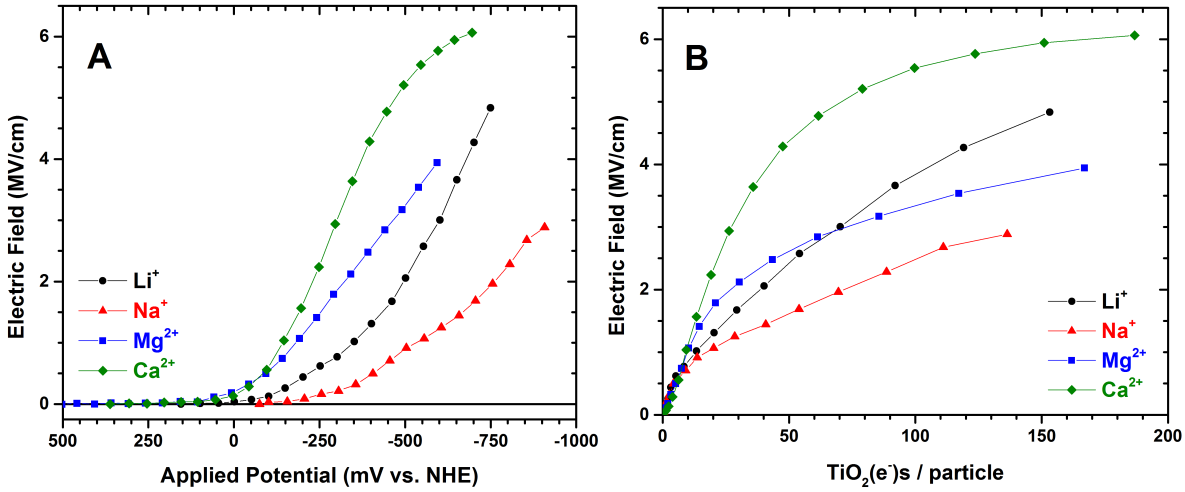

Figure 4.4. Electric field experienced by $Ru(dtb)_2(dcb)/TiO_2$ in acetonitrile solutions containing 100 mM Li^+, Na^+, Mg^{2+}, or Ca^{2+} as a function of: (A) the applied potential and (B) the number of $TiO_2(e^-)$s on a per particle basis.

The relative injection yields were measured by comparative actinometry 100 ns after pulsed 532 nm light excitation of $Ru(dtb)_2(dcb)/TiO_2$ in 100 mM metal perchlorate acetonitrile solutions.[168] The yields were within experimental error unity for Li^+, Mg^{2+}, and Ca^{2+} and found to be 0.95 for Na^+.

Pulsed light excitation into the MLCT absorption band of $Ru(dtb)_2(dcb)/TiO_2$ thin films immersed in 100 mM metal perchlorate solutions with 250 mM of tetrabutylammonium iodide, present to regenerate the sensitizer, generated long-lived charge separated states,

comprised of $TiO_2(e^-)$s and triiodide. Representative transient absorption spectra shown in Figure 4.4 were obtained 2.5 μs after laser excitation, a delay time chosen to ensure that all sensitizers had been regenerated and all iodide oxidation chemistry was complete. The transient absorption spectra exhibit: (1) small absorption features from 400 – 425 nm, attributed to formation of triiodide; (2) a first-derivative shaped feature centered around 485 nm, attributed to the $TiO_2(e^-)$-induced Stark effect; and (3) absorption from 600 – 750 nm, attributed to $TiO_2(e^-)$s. The transient absorption spectra were modeled with first-derivatives of the ground-state absorption spectra, shown in Figure A4.6 in the Appendix, and the electric fields calculated using Equation 4.5 are collected in Table 4.2.

Single-wavelength absorption changes monitored at wavelengths characteristic for $TiO_2(e^-)$s and the Stark effect were quantified over seven orders of magnitude, from 100 ns to 1 s, shown in Figure 4.6. Care was taken to adjust the incident irradiance such that the long wavelength absorption measured 2.5 μs after the laser excitation was the same for all the sensitized materials, such that the number of $TiO_2(e^-)$s was constant. The observed kinetics were non-exponential, but well-modeled by the Kohlrausch-Williams-Watts (KWW) stretched exponential function:

$$I(t) = I_0 \exp[(-kt)^{\beta}] \tag{4.7}$$

where I_0 is the initial amplitude, k is a characteristic rate constant, and β is inversely proportional to the width of an underlying Lévy distribution of rate constants, $0 < \beta < 1$.[176, 195] The data were fit with β fixed to a value of 0.2 and the abstracted rate constants were $k_{Li+,\ Na+} = 5 \times 10^4\ s^{-1}$ and $k_{Mg2+,\ Ca2+} = 5 \times 10^2\ s^{-1}$.

Table 4.2. Ionic Radii, Spectral Shifts, and Electric Field Strength for $Ru(dtb)_2(dcb)/TiO_2$.

Cation	Ionic Radii (Å)[a]	Electrochemically Accumulated $TiO_2(e^-)$s[b]	Photoinjected $TiO_2(e^-)$s[c]	
		Electric Field (MV/cm)	$\Delta\nu$ (cm^{-1})	Electric Field (MV/cm)
Li^+	0.76	1.3	53	0.66
Na^+	1.02	1.1	22	0.28
Mg^{2+}	0.72	1.8	78	0.98
Ca^{2+}	1.00	2.2	30	0.38

[a]Ionic radii obtained from Shannon, Ref [196]. [b] Electric field change measured after the potentiostatic injection of approximately 20 $TiO_2(e^-)$ per nanoparticle. [c]Change in electric field measured 2.5 μs after pulsed laser excitation.

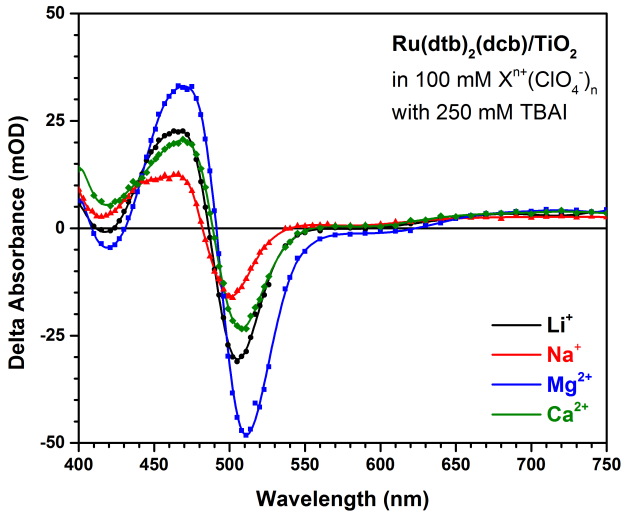

Figure 4.5. Transient absorption spectra obtained 2.5 μs after pulsed 532 nm excitation of $Ru(dtb)_2(dcb)/TiO_2$ in acetonitrile electrolyte solutions containing 100 mM of the indicated perchlorate salts and 250 mM tetra-*n*-butylammonium iodide.

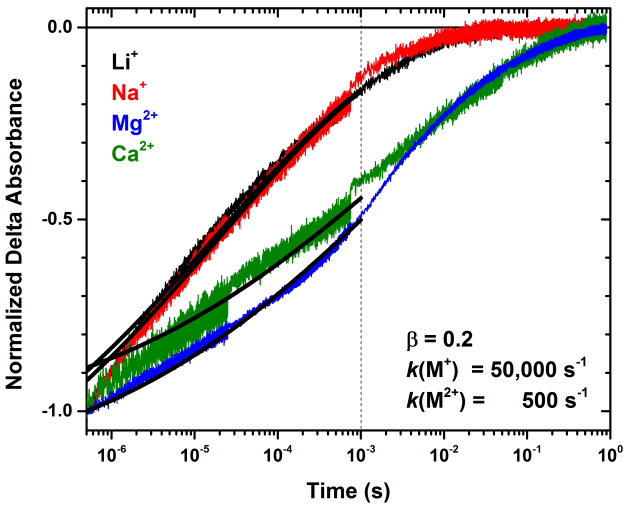

Figure 4.6. Single-wavelength transient absorption kinetic data of $Ru(dtb)_2(dcb)/TiO_2$ in acetonitrile electrolyte solutions containing 100 mM of the indicated perchlorate salts with 250 mM tetra-*n*-butylammonium iodide observed at the maximum of the Stark effect bleach, ~500-510 nm. Overlaid in black are fits to the KWW function.

The nature of the cations present in 100 mM acetonitrile electrolytes surrounding a $Ru(dtb)_2(dcb)/TiO_2$ sensitized thin film were varied to test whether they had an influence on the surface electric field and the dynamics of interfacial charge screening. This was indeed realized and both the kinetics and the electric field were found to be acutely sensitive to the nature of the cation. As is often found to be the case in studies of sensitized materials, the alteration of this one cation variable influenced many properties of the sensitized material

including the interfacial energetics and hence the excited state injection yields. The plausible origin(s) of these spectral changes are described first followed by a description of the electric fields and charge screening dynamics.

4.3.1 – Cation Dependent Interfacial Redox Properties.

The adsorption of ions on semiconductor surfaces is known to have a strong influence on the valence and conduction band edge positions. A well-documented example for metal oxide semiconductors in aqueous solution is the 59 mV shift of the band edges that accompanies a factor of ten change in the proton concentration.[189, 197-198] The surface adsorption of alkali and alkaline earth metal cations can have similar effects and are hence sometimes referred to as 'potential determining ions'.[136, 199-201] In general, cation adsorption shifts the band edge positions positively on an electrochemical scale away from the vacuum level. High efficiency dye-sensitized solar cells (DSSCs) utilize anatase TiO_2 in non-aqueous solvents, very often CH_3CN, where dramatic energetic shifts have been reported. For example, the conduction band edge position has been reported to be -2.1 V vs. SCE in 1.0 M $TBAClO_4$, where the tetrabutylammonium (TBA) cation was reasonably asserted to interact only weakly with the TiO_2 surface, and shifted 1.1 V positive when Lewis acidic Li^+ cations were present.[199] Similar shifts have been reported in other non-aqueous solutions.[200, 202] The cation concentration dependence of these shifts is often non-linear and generally one needs to determine the values experimentally under conditions most relevant to the DSSC.

Spectro-electrochemistry has been widely utilized to characterize the acceptor states of the mesoporous anatase TiO_2 thin films used in DSSCs.[43, 192, 203] Reduction of TiO_2 results in a black coloration as well as a blue shift of the fundamental absorption. For a given cation, the measured spectra were normalizable over the potential range that was investigated, 0.0 to -1.0 V vs. NHE. The extinction coefficients were calculated from the measured absorption spectra and the amount of charge present in the film as was determined by the charge extraction technique of un-sensitized TiO_2.[190-192] The value measured at 700 nm of $\varepsilon = 930 \pm 50\ M^{-1}\ cm^{-1}$ were within experimental error the same and in good agreement with previously published values, Figures A4.1-A4.3 in the Appendix.[10, 192, 202]

While the coloration associated with TiO_2 reduction is well known, an assignment of the underlying electronic transition(s) is not. The blue shift of the fundamental absorption has been attributed to both an electric field[181, 204-205] and a band – filling, i.e. a Burstein-Moss